

NASA Technical Paper 1122

# Simplified Sonic-Boom Prediction

Harry W. Carlson  
*Langley Research Center*  
*Hampton, Virginia*



National Aeronautics  
and Space Administration

**Scientific and Technical  
Information Office**

1978



## SUMMARY

A simplified method for the calculation of sonic-boom characteristics for a wide variety of supersonic airplane configurations and spacecraft operating at altitudes up to 76 km has been developed. Sonic-boom overpressures and signature duration may be predicted for the entire affected ground area for vehicles in level flight or in moderate climbing or descending flight paths. The outlined procedure relies to a great extent on the use of charts to provide generation and propagation factors for use in relatively simple expressions for signature calculation. The computational requirements can be met by hand-held scientific calculators, or even by slide rules. With little sacrifice in accuracy, complete calculations can often be obtained in less time than is required for the preparation of computer input data for the more rigorous calculation methods. A variety of correlations of predicted and measured sonic-boom data for airplanes and spacecraft serve to demonstrate the applicability of the simplified method.

## INTRODUCTION

As the understanding of sonic-boom phenomena has advanced, and the ability to provide accurate predictions of sonic-boom phenomena has improved, the actual prediction process has become quite complex. For conventional airplane configurations, the usual procedures as described in references 1 and 2 call for employment of several sophisticated computer programs covering airplane geometry and aerodynamic considerations as well as the wave propagation aspects of the problem. For spacecraft operating in the sensible atmosphere, it has become the practice (ref. 3) to rely on wind-tunnel tests of small but detailed scale models and specialized computer programs for extrapolation of the data to full-scale conditions. In either case, the process is complex, lengthy, and expensive and requires the services of one or more skilled practitioners of the art.

The results of a recent study indicate that for many purposes (including the conduct of preliminary engineering studies and the preparation of environmental impact statements), sonic-boom predictions of sufficient accuracy can be obtained by using a simplified method which does not require a wind tunnel or elaborate computing equipment. Computational requirements can in fact be met by hand-held scientific calculators, or even slide rules. In addition, successful use of the method is not highly dependent on the skill and knowledge of the person performing the calculations.

This prediction technique results from a simplification of the purely theoretical methods described in references 1 and 2, which have been shown to provide quite acceptable estimates of sonic-boom phenomena for a wide range of flight conditions for conventional airplane configurations. A recent wind-tunnel study (ref. 4) has shown that purely theoretical methods may be applied to prediction of sonic-boom phenomena for extremely blunt bodies at high supersonic speeds, provided that propagation distances are large relative to

body dimensions. This finding justifies the use of the simplified method for spacecraft as well as for conventional airplane configurations.

This report gives a general description of the prediction method, lists the steps required in the calculation procedure, and provides charts that are needed in the process. In addition, sample problems are presented to illustrate the method in use, and correlations with flight-test experimental data are shown to demonstrate its applicability.

The reader interested only in prediction of ground-track overpressures for conventional airplane configurations may wish to go directly to the section entitled "Further Simplification," in which a brief, self-contained prediction method is described.

## SYMBOLS

$A(x)$	area of aircraft cross sections normal to flight direction at a given value of x-coordinate (cross sections normal to longitudinal axis of aircraft may be substituted in most cases), $m^2$
$A_e(x)$	total effective area of aircraft at a given value of x-coordinate, $A(x) + B(x)$ , $m^2$
$A_{e,max}$	maximum effective area, $m^2$
$A_{e,1}$	total effective area at midpoint of effective aircraft length, $l_e$ , $m^2$
$a_v$	speed of sound at aircraft (vehicle) altitude, m/sec
$B(x)$	equivalent cross-sectional area due to lift at a given value of x-coordinate, $m^2$
$B_{max}$	maximum equivalent cross-sectional area due to lift, $m^2$
$b(x)$	local span of aircraft planform at a given value of x-coordinate, m
$d$	distance between aircraft ground-track position at time of sonic-boom generation and location of ground impact point (see fig. 5), km
$d_x$	component of $d$ in direction of aircraft ground track, km
$d_y$	component of $d$ in a direction perpendicular to aircraft ground track (i.e., in lateral direction), km
$d_{y,c}$	value of $d_y$ at lateral limit or cutoff of sonic-boom ground footprint, km
$h$	altitude of aircraft above ground, $h_v - h_g$ , km

$h_e$	effective altitude (see fig. 5), km
$h_g$	altitude of ground above sea level, km
$h_v$	altitude of aircraft (vehicle) above sea level, km
$K_d$	ray-path distance factor
$K_{d,c}$	ray-path distance factor for cutoff conditions, $M_e = M_c$
$K_{d,\infty}$	ray-path distance factor for an infinite Mach number
$K_L$	lift parameter (see fig. 4)
$K_p$	pressure amplification factor
$K_{p,\infty}$	pressure amplification factor for an infinite Mach number
$K_R$	reflection factor, assumed to be 2.0
$K_S$	aircraft shape factor
$K_t$	signature duration factor
$K_{t,\infty}$	signature duration factor for an infinite Mach number
$l$	aircraft characteristic length, normally the fuselage length, m
$l_e$	effective length of aircraft used in determination of aircraft shape factor, m
$M$	aircraft Mach number
$M_c$	aircraft cutoff Mach number below which sonic boom will not reach ground
$M_e$	aircraft effective Mach number governing sonic-boom atmosphere propagation characteristics
$n_d$	exponent of Mach number parameter in atmospheric distance factor curve fit (see eq. (12))
$n_p$	exponent of Mach number parameter in atmospheric pressure amplification factor curve fit (see eq. (13))
$n_t$	exponent of Mach number parameter in atmospheric signature duration factor curve fit (see eq. (14))
$p$	atmospheric pressure, Pa
$\Delta p$	incremental pressure due to sonic boom, Pa

$\Delta p_{\max}$	incremental pressure at N-wave bow shock, also referred to as bow-shock overpressure, Pa
$p_g$	atmospheric pressure at ground level, Pa
$p_v$	atmospheric pressure at aircraft (vehicle) altitude, Pa
$S$	aircraft planform area, $m^2$
$\Delta t$	time increment, sec
$W$	aircraft weight, kg
$x$	distance from aircraft nose measured backward along flight path, m
$\gamma$	flight-path angle (see fig. 5), deg
$\theta$	ray-path azimuth angle (see fig. 5), deg
$\phi$	angle between aircraft ground track and ground projection of ray path (see fig. 5), deg

#### METHOD IN GENERAL

The simplified prediction method is applicable to a wide variety of supersonic airplane configurations and spacecraft operating at altitudes up to 76 km. It provides estimates of sonic-boom pressure and signature duration over the entire exposed ground area for vehicles in level flight or in moderate climb or descent flight profiles. The effects of flight-path curvature and aircraft acceleration, however, are not considered, and the method is further restricted to a standard atmosphere without winds. These limitations, however, do not appear to affect the general applicability of the method for normal variations from the standard atmosphere (temperature profiles and winds) and for moderate flight-path curvature and aircraft acceleration. When situations do arise in which these effects are important, Whitham F-function data provided by the simplified method may be used to supply sonic-boom generation data necessary for employment of the propagation computer program described in reference 5.

Another possible restriction to the general applicability of the simplified method is the assumption that the pressure signal generated by the aircraft is of the far-field type, the classical N-wave (a compression or shock wave followed by a linear expansion to pressures below ambient and a second shock of equal magnitude which restores ambient pressure). Normally this is a valid assumption, at least for the bow shock and the positive portion of the signature, and even when near-field effects become noticeable (some examples are shown) the estimate provided by the simplified method tends to be conservative.

The information required for the calculations and the pressure-signature predictions provided by the simplified method may be discussed with the aid of

figure 1. First, the factors governing the generation of the sonic boom must be known. For aircraft not covered by shape-factor charts provided in this report, a general description of the aircraft geometry must be provided so that shape factors may be calculated. The description need not be detailed, and no knowledge of the aircraft lift distribution is required. Of course, the aircraft operating conditions - Mach number, altitude, weight, and flight-path angle - must be known. In addition, atmospheric pressure and sound speed at the aircraft altitude and at ground level must be known. The signature data provided by the method include the N-wave bow-shock pressure rise, the signature duration, and the location of the ground impact point relative to the aircraft position at the time the boom was generated.

The procedure for calculation of sonic boom by the simplified method involves three basic steps: determination of an aircraft shape factor, evaluation of atmospheric propagation factors, and calculation of signature shock strength and duration. These basic steps are implemented as follows:

(1) Determine aircraft shape factor  $K_S$

- (a) From the aircraft geometry, calculate  $K_S$  for a specified weight and set of operating conditions according to the steps outlined in the section "Shape-Factor Calculation"

or

- (b) For aircraft covered by the charts discussed in the section "Shape-Factor Charts," use aircraft weight and operating conditions to calculate lift parameter and read  $K_S$  directly.

(2) Determine propagation parameters  $M_e$  and  $h_e$  from the operating conditions according to equations given in the section "Atmospheric Factor Derivation," and read atmospheric factors  $K_p$  and  $K_t$  from the charts discussed in the section "Atmospheric-Factor Charts."

(3) Calculate bow-shock overpressure from the equation

$$\Delta p_{\max} = K_p K_R \sqrt{p_v p_g} (M^2 - 1)^{1/8} h_e^{-3/4} l^{3/4} K_S \quad (1)$$

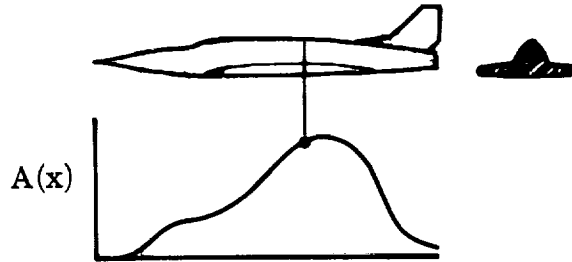
and signature duration from the equation

$$\Delta t = K_t \frac{3.42}{a_v} \frac{M}{(M^2 - 1)^{3/8}} h_e^{1/4} l^{3/4} K_S \quad (2)$$

## SHAPE-FACTOR CALCULATION

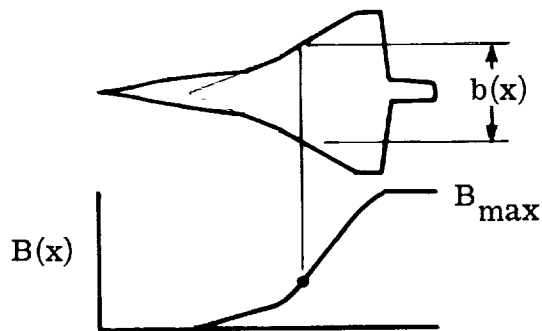
The computer method of reference 6 has been considerably simplified to obtain the following procedure for calculation of aircraft shape factor from geometric data.

The first step, the definition of aircraft cross-sectional areas, requires only areas normal to the flight path (except for very large angles of attack, areas normal to the aircraft longitudinal axis are equally acceptable) rather than those defined by Mach planes. A typical distribution obtained in this manner is shown in the following sketch:



Little loss of accuracy results from this simplification; there is, in fact, evidence that for blunt shapes or high supersonic speeds the normal areas are more appropriate (ref. 4). Although some care should be taken in establishing the maximum cross-sectional area and its location, great precision is not required and only the general shape of the remainder of the curve need be of concern. If known, the area of the stream tube of air entering the engine inlet should be subtracted from the total defined by external contours.

The second step involves the definition of an equivalent area due to lift. Detailed theoretical methods of deriving this contribution are discussed in references 1 and 6. It has been found that a reasonably accurate approximation of the lift distribution may be defined by the planform area distribution as illustrated in the following sketch:



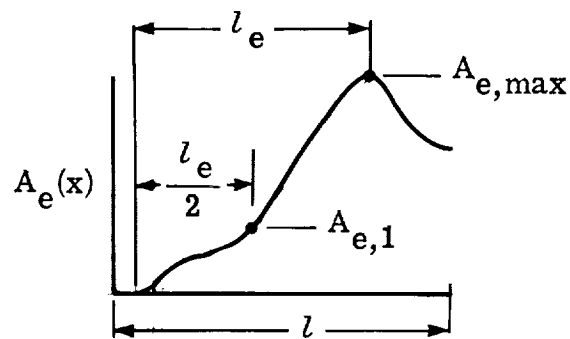


The equivalent area due to lift is defined by the equation

$$B(x) = \frac{\sqrt{M^2 - 1} W \cos \gamma \cos \theta}{1.4 p_\infty M^2 S} \int_0^x b(x) dx$$

Note that the lifting force which influences the sonic boom is defined by an aircraft weight component normal to the flight path and directed along the initial ray-path azimuth angle  $\theta$ .

The third step is the combination of these two area contributions to obtain a distribution for the total effective area of the aircraft, illustrated in the following sketch:



From this curve, the maximum effective area  $A_{e,max}$  and its location can be determined. Then, as shown in the sketch, the effective length  $l_e$  and the effective area  $A_{e,1}$  required for evaluation of the aircraft shape factor may be selected.

Finally, in the fourth step, the aircraft shape factor may be found from a reading of the shape-factor parameter curve of figure 2 and insertion of the appropriate areas and lengths. The shape-factor parameter has been defined by evaluation of sonic-boom theory for an effective area distribution of the form  $A_e(x) = k_1 x + k_2 x^2$ , with constants  $k_1$  and  $k_2$  selected so the curve passes through the  $A_{e,1}$  and  $A_{e,max}$  points. (See sketch at top of fig. 2.) Note that the aircraft shape factor is primarily dependent on the maximum effective area. The location of the maximum area and the shape of the effective area development play lesser roles.

The ability of the simplified procedure to account for shape-factor variation of a representative supersonic airplane is illustrated in figure 3. Effective area developments shown in the figure cover the extremes and the midpoint of lift parameters likely to be encountered in normal flight. Signatures shown below each of the effective area developments indicate the influence of the shape-factor variation on the signature characteristics. As can be seen in equations (1) and (2), both overpressure and duration vary directly with the magnitude of the shape factor. It has been found that the simplified

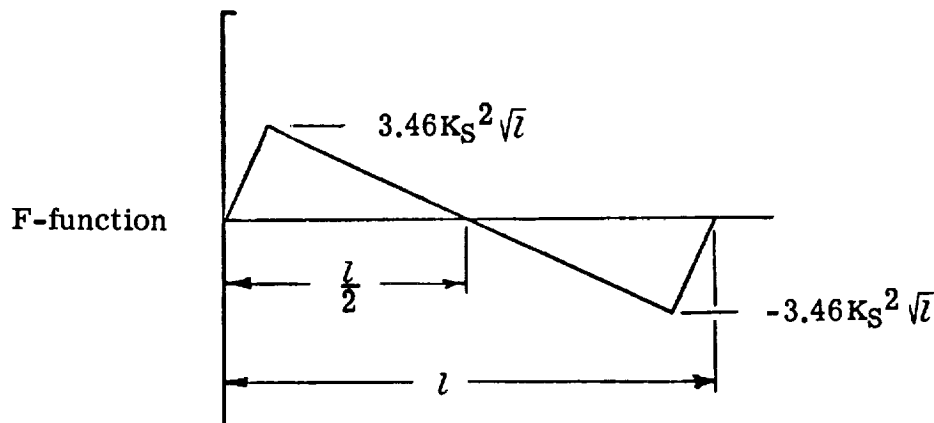
curve-fit method gives shape factors which are generally within 5 percent (and almost always within 10 percent) of the values given by the more rigorous theoretically based computer methods.

### SHAPE-FACTOR CHARTS

For the reader's convenience, aircraft shape factors for a variety of airplanes employed in sonic-boom flight-test programs and for more contemporary aircraft are given in the charts of figure 4. To use these charts it is necessary only to identify the aircraft of concern, calculate the lift parameter  $K_L$ , and read the shape factor directly. Note that with the exception of the space shuttle orbiter, which is set apart as a result of its high volume, shape factors for all the aircraft fall in a fairly narrow band. For aircraft not specifically covered by the charts, shape factors may be chosen by selecting a similar configuration. Generally, larger airplanes are more slender and will have lower shape factors. Fighter airplanes, on the other hand, tend to have higher shape factors. At the upper end of the lift-parameter range, the shape factor is more dependent on the wing planform than on the aircraft size and volume, and highly swept wings tend to have better shape factors.

There is no great sensitivity of the final overpressure and duration calculations to the choice of the aircraft characteristic length  $l$ , even though it appears as a squared term in the lift parameter. It is important, however, that the chosen length be used consistently throughout the calculations.

If, as mentioned in the introduction, it becomes necessary to consider the effects of curved flight paths and acceleration in situations where far-field conditions are to be expected, the shape factor provided by this simplified prediction method may be used to supply an input F-function for the atmospheric propagation program of reference 5. The necessary F-function may be represented by a double triangular distribution as shown in the following sketch:



Definition of the lifting force normal to the flight path used in shape-factor determination must now include the effects of aircraft accelerations; it is no longer appropriate to use only a component of the aircraft weight as is done throughout this report.

#### ATMOSPHERIC-FACTOR DERIVATION

Atmospheric propagation factors for ray-path distance, pressure amplification, and signature duration have been derived from repeated use of the sonic-boom propagation computer program described in reference 5 for a matrix of altitudes, Mach numbers, ray-path azimuth angles, and flight-path angles. To determine these factors, the program was run first with a standard atmosphere, and then with a uniform atmosphere with a pressure equal to the geometric mean of the standard atmospheric pressures of the aircraft altitude and at ground level,  $\sqrt{p_v p_g}$ . The factors are simply the ratios of sonic-boom parameters given by the first run to those given by the second.

In order to broaden the applicability of the atmospheric propagation factors and allow the use of on-track and level-flight data for off-track and flight-path-angle conditions, the concepts of effective Mach number and effective altitude were employed. It was presumed that the ray-path curvature and the overpressure amplification due to atmospheric effects would depend primarily on the initial inclination of the aircraft-generated ray path with respect to the earth plane and on the ray-path distance measured perpendicular to the aircraft flight path. A convenient measure of the ray-path inclination is the Mach number for level flight, which would have the same ray-path angle in the flight-track plane. This is termed the effective Mach number. The ray-path distance measured perpendicular to the aircraft flight path is termed the effective altitude. Geometric relationships used in the derivation of these parameters are illustrated in figure 5. Simplified equations for effective Mach number, propagation distance, and effective altitude for the on-track case are as follows:

$$M_e = \frac{1}{\sin \left( \gamma + \cot^{-1} \sqrt{M^2 - 1} \right)} \quad (3)$$

$$d_x = K_d \left( \frac{h}{\sqrt{M_e^2 - 1}} \right) \quad (K_d \text{ from fig. 7(b)}) \quad (4)$$

$$h_e = h \cos \gamma + d_x \sin \gamma \quad (5)$$

Complete equations for the more general off-track case are as follows:

$$M_e = \sqrt{1 + \frac{\left[ \frac{1}{\cos \gamma \sqrt{M^2 - 1}} \left( 1 - \frac{\tan \gamma}{\cos \theta \sqrt{M^2 - 1}} \right) \right]^2}{\left[ \left( \tan \gamma + \frac{1}{\cos \theta \sqrt{M^2 - 1}} \right) \frac{1}{\cos \gamma \sqrt{M^2 - 1}} \right]^2 + \left[ \frac{\tan \theta}{\sqrt{M^2 - 1}} (\tan^2 \gamma + 1) \right]^2}} \quad (6)$$

$$d = K_d \left( \frac{h}{\sqrt{M_e^2 - 1}} \right) \quad (7)$$

$$\phi = \tan^{-1} \frac{\tan \theta \cos \gamma (1 + \tan^2 \gamma)}{\tan \gamma + \frac{1}{\cos \theta \sqrt{M^2 - 1}}} \quad (8)$$

$$d_x = d \cos \phi \quad (9)$$

$$d_y = d \sin \phi \quad (10)$$

$$h_e = \sqrt{d_y^2 + (h \cos \gamma + d_x \sin \gamma)^2} \quad (11)$$

The usefulness of the effective Mach number and effective altitude in reducing a large amount of computer-generated data to manageable proportions is illustrated in figure 6. For a selected altitude of 20.0 km, ray-path distance factor  $K_d$  and pressure amplification factor  $K_p$  are shown as a function of the effective Mach number. The Mach number scale was chosen in order to cover Mach numbers from one to infinity with an expansion of the lower Mach number range. Program-generated data are given for ray-path azimuth angles from  $0^\circ$  to  $60^\circ$  and for flight-path angles from  $-15^\circ$  to  $30^\circ$ . The nesting of the data verifies the concepts of the effective Mach number and the effective altitude. For other altitudes up to about 70 km, the tendency toward collapse of the data to a single line is generally somewhat more pronounced than that shown in figure 6.

#### ATMOSPHERIC-FACTOR CHARTS

Atmospheric factors required in this simplified method for sonic-boom prediction are presented in figure 7. The first chart (fig. 7(a)) gives the cutoff Mach number in a standard atmosphere as a function of aircraft altitude. Cutoff occurs for disturbances which propagate away from the aircraft along a

ray path (as defined by the effective Mach number) which curves under the influence of atmospheric gradients to an extent just sufficient for it to become horizontal at ground level. As is discussed later, this cutoff limits the lateral extent of the ground area affected by the sonic boom. If the effective Mach number calculated according to the appropriate equation from the preceding section is not greater than the cutoff Mach number for the aircraft altitude, there is no need to go further; the signal will not reach the ground.

Ray-path distance factors are given in figure 7(b). The horizontal distance traveled by a particular ray path from the time a signal leaves the aircraft until it reaches the ground may be found by using this factor. The factor read from the chart for a given altitude and effective Mach number is simply multiplied by the distance traveled in a uniform atmosphere

$\left( h / \sqrt{M_e^2 - 1} \right)$ . Interpolation must be done with care because of the nonlinear nature of the data. There is no need to use the ray-path distance-factor charts for estimates of level-flight on-track overpressure; they are required, however, to obtain an effective altitude for overpressure calculation at off-track locations and for flight-path angles other than zero.

The limiting or cutoff ray-path distance factor may be read from figure 7(c). The primary use of this chart is in defining the lateral extent  $d_{y,c}$  of the affected ground area for level flight given by

$$d_{y,c} = K_{d,c} \frac{h}{M} \sqrt{\frac{M^2 - M_c^2}{M_c^2 - 1}}$$

The chart is also useful in defining the sonic-boom footprint limits for moderate climbing or descending flight profiles. These limits, however, must be found by iteration. The cutoff distance chart was prepared from an analysis given in reference 7. The computer program of reference 5 does not provide this information since calculations are terminated when ray paths come within  $2^\circ$  of the horizontal.

Pressure amplification factors are presented in figure 7(d). Care is required for accurate interpolation of the charts because of the nonlinear nature of the data. This factor, in combination with the effective-altitude term, accounts for nonuniform atmospheric effects in the equation for bow-shock overpressure given in equation (1).

The final atmospheric-factor chart (fig. 7(e)) gives the signature duration factor which, in combination with the effective-altitude term, accounts for the effects of a nonuniform atmosphere in the equation for signature duration given in equation (2). The actual Mach number rather than the effective Mach number is used when reading this chart.

The atmospheric-factor charts presented herein apply directly to the situation where ground level is at or near sea level. The charts can, however,

be used with little error for ground levels up to about 1600 meters. The aircraft altitude above sea level  $h_v$  should be used when entering the charts, and the altitude above ground level  $h$  should be used when calculating the effective altitude and propagation distances.

Generally, the atmospheric propagation factors may be read directly from the previously discussed charts. However, the charts which cover only Mach numbers greater than 1.2 do not give sufficient information for situations in which cutoff conditions are approached. To cover these situations, the following curve-fit equations which employ exponents given in figure 8 may be used:

$$K_d = K_{d,c} + (K_{d,\infty} - K_{d,c}) \left( \frac{M_e - M_c}{M_e - 1} \right)^{n_d} \quad (12)$$

$$K_p = K_{p,\infty} \left( \frac{M_e - 1}{M_e - M_c} \right)^{n_p} \quad (13)$$

$$K_t = K_{t,\infty} \left( \frac{M}{M - 1} \right)^{n_t} \quad (14)$$

The form of these curve-fit equations was suggested by the nature of the program data as exemplified in figure 6. The asymptotic approach of the factors to limiting values at Mach numbers approaching infinity should be noted. The pressure factor displays singular behavior as the cutoff Mach number is approached, but the distance factor has a finite limit at this Mach number. These characteristics were taken into account in the formulation of the curve fit. An example of the curve-fit approximation is given in figure 6.

Equations (12) to (14) and the exponent curves of figure 8 appear to be somewhat formidable. The information, however, may be employed in a rather straightforward manner. First, it is necessary to define the cutoff Mach number and limiting values of the atmospheric factors from figure 7. Then, for the given altitude, read the curve-fit exponents for each of the three factors from the chart of figure 8. Finally, find the atmospheric factors by substituting the desired effective Mach number, the cutoff Mach number, the limiting factors, and the curve-fit exponents into equations (12) to (14).

#### SIGNATURE CALCULATION

In the preceding sections, means of obtaining an aircraft shape factor were described and the procedure for reading atmospheric propagation factors from the charts was outlined. In the process of evaluating the atmospheric propagation factor, the location of the impact point on the ground relative to

the position of the aircraft at the time of generation ( $d_x$  and  $d_y$ ) is also provided.

With the shape factors and atmospheric factors in hand, the signature may be calculated by applying equations (1) and (2). All the terms are described in the section "Symbols" and some are discussed in detail elsewhere in this report.

It may be of help here to discuss the reflection factor  $K_R$ . When the shock wave meets the Earth, flow velocities behind the shock are altered; vertical velocities are blocked and their energy is converted into a pressure increase. For weak shocks meeting a smooth, rigid, and flat surface, the resultant overpressure is theoretically twice that of the free-air value of the incident wave. In flight tests, reflection factors varying from about 1.8 to 2.0 have been recorded. The lower values are generally associated with sandy or marshy terrain. For ground overpressure predictions presented in this report, a reflection factor of 2.0 has been assumed.

Although the calculative procedures are relatively straightforward and simple, it may be desirable to utilize the programming capabilities of some of the modern pocket-sized or desk-top calculators for repetitive calculations. Some notes on programming are offered in appendix A.

A series of three sample problems has been prepared to aid the reader in understanding the calculation process. These problems are presented in appendix B.

#### CORRELATION WITH FLIGHT-TEST DATA

To demonstrate the applicability of the simplified sonic-boom prediction method to a variety of problems, correlations with flight-test data (refs. 8 to 14) are shown in figures 9 to 13.

In figure 9, predictions are compared with measured signatures for three distinct airplane types (refs. 8 and 9) operating at or near cruise conditions. Only for the fighter aircraft, which displays some evidence of near-field effects, is there an appreciable difference between predicted and experimental results. In this situation, as noted previously, the prediction is conservative.

Correlations of predictions with measurements for a reconnaissance airplane (ref. 10) covering a range of flight altitudes are shown in figure 10. The variation of  $\Delta p_{\max}$  with  $h_v$  is quite typical of that for most airplanes; the Mach number differences are of secondary importance.

The validity of the method for off-track predictions for a bomber airplane (ref. 8) is illustrated in figure 11. At large lateral distances, the ray paths curve sufficiently to approach the Earth at near-grazing angles. This results in signature distortions and ultimately in a breakup of a recognizable signature into random noise beyond the lateral cutoff. There is some evidence of such a transition for the most distant signature shown in the

figure. In general, the variations with lateral distance are predicted reasonably well; however, there is a singularity predicted at the cutoff point which does not appear to materialize. Other examples of measured lateral-spread patterns are given in reference 15. No evidence of pressure amplification at the cutoff point is shown in reference 15, and the authors apparently have chosen to fair the prediction curve in a monotonically decreasing fashion rather than attempt to define the theoretical singularity. Users of this system may choose to do likewise.

It is remarkable that the predictions for the Apollo command modules shown in figure 12 bear any similarity to the measured data (refs. 11 and 12). The diameter-length ratio of the effective body shape is about 9 and the effective length is only 0.42 m. The appearance of the unexpected multiple shocks in the measured signatures remains unexplained. Although the correlations are far from exact, the predictions are nevertheless useful. Especially notable is the degree of correlation indicated for a Mach number of 15.

Another example of the applicability of the simplified prediction method to spacecraft is given in figure 13. As mentioned in the discussion of the sample problems (appendix B), the sonic boom generated by the Apollo launch vehicles (refs. 12 and 13) is dominated by the exhaust gas plume, so this is a very special situation. Another special feature is the ground pattern of the signatures. As shown in the flight-path profile there are two families of rays. One family consists of near-grazing rays generated prior to generation of that ray which reaches a point nearest the launch. The other family consists of more direct rays generated after that time. As can be seen on the plot of overpressure versus distance from launch, there is a portion of the ground track over which double or superimposed signatures are predicted. It is apparent from the inset pressure-signature sketches that the grazing-ray component of these signatures is grossly overpredicted. However, the pressure-doubling at the closest ground intersection point appears to have materialized. Large distances traveled in proximity to the Earth appear to cause disintegration of a distinct signature into random noise. There is also a question as to whether grazing rays should be considered to have a surface reflection factor of 2 or a free-air reflection factor of 1. These data seem to indicate that the grazing-ray pressure signatures should be ignored. However, at the first ground-track point, members of the grazing-ray family have not yet reached grazing conditions and thus contribute to the signature. With this stipulation, the predicted overpressure indicated by the solid line agrees reasonably well with the measured data. The predicted signature duration, however, as indicated by the sketches, is too large by a factor of nearly 2. The curved flight path and the vehicle acceleration may play some part in the cause of the discrepancy.

#### FURTHER SIMPLIFICATION

For readers interested only in prediction of on-track overpressure for conventional airplane configurations, several of the steps in the general simplified method may be omitted. In this case it is possible to place all the necessary information, with the exception of atmospheric tables, on a single page. This "super simplified" method is given in figure 14.



Predictions obtained by this method are compared with flight-test data for three airplanes (refs. 8 and 14) in figure 15. Each prediction is shown as a band to account for variations in airplane weight and Mach number that occur at a given altitude. Deviations of predictions from measurements occur at the lower altitudes for both the large bomber and the small fighter. These differences arise because the simplified methods do not account for the presence of a small amount of near-field effect in the signatures generated by these airplanes. Such discrepancies are anticipated for very large and slender airplanes, but the measured signatures for the small fighter are not at all typical of fighter aircraft. The near-field effect for the fighter is due to the nontypical long slender nose. A redeeming quality of the prediction method is that when near-field effects do occur, the prediction tends to be conservative.

#### CONCLUDING REMARKS

A simplified method for calculation of the sonic-boom characteristics of greatest interest for a wide variety of airplane configurations and spacecraft has been described. The procedure, which has been outlined in a step-by-step manner, relies to a great extent on the use of charts to provide the necessary sonic-boom generation and propagation factors for use in relatively simple expressions for signature characteristics. Computational requirements can be met by hand-held scientific calculators or by slide rules. With little sacrifice in accuracy, complete calculations can often be obtained in less time than is required for the preparation of computer input data for the more rigorous calculation methods. A variety of correlations of predicted and measured sonic-boom data for airplanes and spacecraft serve to demonstrate the applicability of the method.

Langley Research Center  
National Aeronautics and Space Administration  
Hampton, VA 23665  
January 31, 1978

## APPENDIX A

### NOTES ON PROGRAMMING

As was mentioned in the main body of the report, it was found that the computational needs of the simplified sonic-boom prediction method could be met by hand-held scientific calculators. With programmable pocket-sized or desk-top calculators, the labor of performing the calculations can be reduced to an almost negligible level. Some notes on strategy for employment of programmable calculators are offered here.

Before a programmed solution may be employed, it is necessary to have shape-factor charts for the aircraft of concern. For aircraft not covered in figure 4, a shape-factor chart may be prepared according to the steps outlined in the section "Shape-Factor Calculation."

It was found to be convenient to calculate the atmospheric factors first. The primary input quantities are the flight conditions  $M$ ,  $\theta$ ,  $\gamma$ , and  $h_v$  and the ground level  $h_g$ . If the curve-fit data are to be used in determination of the atmospheric factors, the quantities  $M_o$ ,  $K_{d,\infty}$ ,  $K_{d,c}$ ,  $K_{p,\infty}$ ,  $K_{t,\infty}$ ,  $n_d$ ,  $n_p$ , and  $n_t$  read from the charts for the flight altitude may also be used as initial input.

The effective Mach number  $M_e$  and the ray-path azimuth angle  $\phi$  may be calculated as follows:

$$M_e = \sqrt{1 + \frac{[A(1 - B \tan \gamma)]^2}{[A(\tan \gamma + B)]^2 + (CD)^2}}$$

$$\phi = \tan^{-1} \left( \frac{\tan \theta \cos \gamma D}{\tan \gamma + A} \right)$$

where

$$A = \frac{1}{\cos \gamma \sqrt{M^2 - 1}}$$

$$B = \frac{1}{\cos \theta \sqrt{M^2 - 1}}$$

$$C = \frac{\tan \theta}{\sqrt{M^2 - 1}}$$

$$D = \tan^2 \gamma + 1$$

## APPENDIX A

With the effective Mach number known, the atmospheric factors may be determined either from a direct reading of the charts (which requires a program temporary stop for chart reading and input of  $K_d$ ,  $K_p$ , and  $K_t$ ) or from the curve-fit data. When evaluating atmospheric factors from the curve-fit data, first test  $M_e$  to see if it is greater than  $M_c$ . If it is not, the calculation must be terminated; the ray path chosen will not reach the ground. To evaluate the atmospheric factors  $K_d$ ,  $K_p$ , and  $K_t$  from the curve-fit data, use the following expressions:

$$K_d = K_{d,c} + (K_{d,\infty} - K_{d,c}) \left( \frac{M_e - M_c}{M_e - 1} \right)^{n_d}$$

$$K_p = K_{p,\infty} \left( \frac{M_e - 1}{M_e - M_c} \right)^{n_p}$$

$$K_t = K_{t,\infty} \left( \frac{M}{M - 1} \right)^{n_t}$$

The ground location of the boom and the effective altitude may now be found as follows:

$$d = \frac{K_d(h_v - h_g)}{\sqrt{M_e^2 - 1}}$$

$$d_x = d \cos \phi$$

$$d_y = d \sin \phi$$

$$h_e = \sqrt{d_y^2 + [(h_v - h_g) \cos \gamma + d_x \sin \gamma]^2}$$

To calculate the magnitude of the sonic-boom overpressure, first evaluate the lift parameter  $K_L$  as follows:

$$K_L = \frac{\sqrt{M^2 - 1} W \cos \gamma \cos \theta}{1.4 p_v M^2 l^2}$$

When  $K_L$  is known, it is necessary to provide another temporary stop for reading and input of the aircraft shape factor from the appropriate curve. In

## APPENDIX A

addition, the quantities  $p_v$ ,  $p_g$ ,  $a_v$ , and  $K_R$  must be input. Now the bow-shock overpressure and the signature duration may be calculated as follows:

$$\Delta p_{\max} = K_p K_R \sqrt{p_v p_g} (M^2 - 1)^{1/8} h_e^{-3/4} l^{3/4} K_S$$

$$\Delta t = K_t \frac{3.42}{a_v} \frac{M}{(M^2 - 1)^{3/8}} h_e^{1/4} l^{3/4} K_S$$

Any consistent set of measurement units may be used as input. The overpressure will be in the units of the atmospheric pressure and the signature duration will be in the time unit used for the speed of sound.

## APPENDIX B

### SAMPLE PROBLEMS

The calculations required for the three sample problems are presented in this appendix with only a brief explanation. The first sample problem illustrates the calculation of the shape factor from aircraft geometric data, in this case taken from small-scale three-view drawings such as those found in reference 16. The calculations shown in the second problem cover the situation in which an aircraft shape factor may be read from the charts. The off-track signature calculation, however, is somewhat more complicated than the on-track calculation of the first sample problem. The third problem covers an unusual situation in which the sonic-boom behavior is dominated by the exhaust gas plume of the propulsion system rather than by the vehicle itself. This problem also demonstrates the versatility of the simplified method. The area of the exhaust gas plume of the ascending Apollo launch vehicle was obtained from data presented in reference 17.

#### Sample Problem 1: Reconnaissance Airplanes, On-Track

The flight conditions and geometric data are

$$\begin{aligned}M &= 1.99 & W &= 41\,000 \text{ kgf} = 402\,000 \text{ N} \\l &= 32.7 \text{ m} & \gamma &= 0^\circ & \theta &= 0^\circ \\h_v &= 15.240 \text{ km} & p_v &= 11.6 \text{ kPa} & a_v &= 295 \text{ m/sec} \\h_g &= 0.760 \text{ km} & p_g &= 92.3 \text{ kPa} & K_R &= 2.0 \\h &= h_v - h_g = 14.480 \text{ km}\end{aligned}$$

The aircraft shape factor is obtained as follows:

$$B_{\max} = \frac{\sqrt{M^2 - 1} W}{1.4 p_v M^2} = 10.7 \text{ m}^2$$

# APPENDIX B

From the area plots at right  
(from data given in ref. 16)

$$l_e = 24 \text{ m}$$

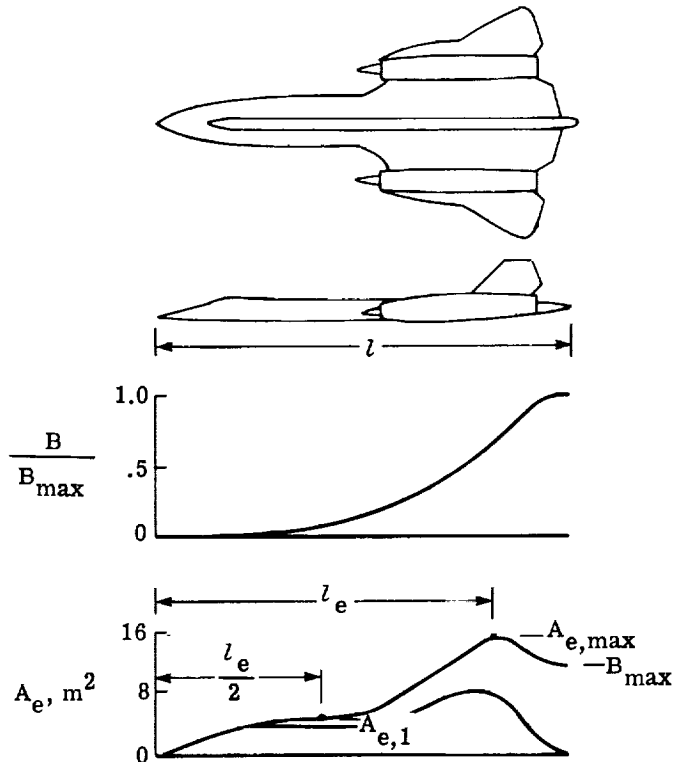
$$A_{e,\max} = 15.0 \text{ m}^2$$

$$A_{e,1} = 4.4 \text{ m}^2$$

$$A_{e,1}/A_{e,\max} = 0.29$$

From figure 2,

$$K_S = 0.685 \frac{\sqrt{A_{e,\max}}}{l^{3/4} l^{1/4}} = 0.087$$



Propagation factors are obtained from equations (3) to (5) and figure 7.

$$M_e = M = 1.99$$

$$h_e = h = 14.480 \text{ km}$$

$$K_p = 1.10$$

$$K_t = 0.85$$

The signature is calculated as follows:

$$\Delta p_{\max} = K_p K_R \sqrt{p_v p_g} (M^2 - 1)^{1/8} h_e^{-3/4} l^{3/4} K_S = 74 \text{ Pa}$$

$$\Delta t = K_t \frac{3.42}{a_v} \frac{M}{(M^2 - 1)^{3/8}} h_e^{1/4} l^{3/4} K_S = 0.17 \text{ sec}$$

# APPENDIX B

## Sample Problem 2: Medium Bomber Airplane, Off-Track

The flight conditions and geometric data are

$$M = 2.0$$

$$W = 36\,000 \text{ kgf} = 353\,000 \text{ N}$$

$$l = 30 \text{ m}$$

$$\gamma = 0^\circ$$

$$\theta = 52^\circ$$

$$h_V = 18.600 \text{ km}$$

$$p_V = 6.88 \text{ kPa}$$

$$a_V = 296 \text{ m/sec}$$

$$h_g = 0.760 \text{ km}$$

$$p_g = 92.3 \text{ kPa}$$

$$K_R = 2.0$$

$$h = h_V - h_g = 17.840 \text{ km}$$

The aircraft shape factor is obtained from figure 4.

$$K_L = \frac{\sqrt{M^2 - 1} W \cos \gamma \cos \theta}{1.4 p_V M^2 l^2} = 0.0108$$

$$K_S = 0.088$$

Propagation factors are obtained from equations (6) to (14) and figures 7 and 8.

$$M_e = \sqrt{1 + \frac{\cos^2 \theta (M^2 - 1)}{1 + \cos^2 \theta \tan^2 \theta (M^2 - 1)}} = 1.182$$

$$d = K_d \left( \frac{h}{\sqrt{M_e^2 - 1}} \right) = 37.4 \text{ km}$$

$$\phi = \tan^{-1} \left( \tan \theta \cos \theta \sqrt{M^2 - 1} \right) = 53.8^\circ$$

$$d_y = d \sin \phi = 30.2 \text{ km}$$

$$h_e = \sqrt{d_y^2 + h^2} = 35.1 \text{ km}$$

# APPENDIX B

$$M_c = 1.153$$

$$K_d = \left( \frac{M_e - M_c}{M_e - 1} \right)^{n_d} (K_{d,\infty} - K_{d,c}) + K_{d,c} = 1.32$$

$$K_p = K_{p,\infty} \left( \frac{M_e - 1}{M_e - M_c} \right)^{n_p} = 1.42$$

$$K_t = K_{t,\infty} \left( \frac{M}{M - 1} \right)^{n_t} = 0.82$$

The signature is calculated as follows:

$$\Delta p_{\max} = K_p K_R \sqrt{p_v p_g} (M^2 - 1)^{1/8} h_e^{-3/4} l^{3/4} K_S = 36.1 \text{ Pa}$$

$$\Delta t = K_t \frac{3.42}{a_v} \frac{M}{(M^2 - 1)^{3/8}} h_e^{1/4} l^{3/4} K_S = 0.19 \text{ sec}$$



## APPENDIX B

### Sample Problem 3: Apollo Launch Vehicle in Ascent

The flight conditions and geometric data are

$M = 4.08$	125 sec and 32.9 km from launch	
$l = 104.5 \text{ m}$	$\gamma = 31.6^\circ$	$\theta = 0^\circ$
$h_v = h = 36.1 \text{ km}$	$p_v = 0.490 \text{ kPa}$	$a_v = 310 \text{ m/sec}$
$h_g = 0$	$p_g = 101 \text{ kPa}$	$K_R = 2.0$

The aircraft shape factor is determined from area plot at right (from data given in ref. 17).

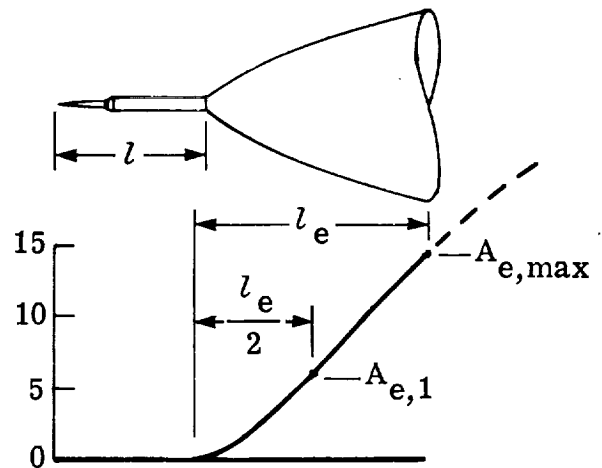
$$l_e = 160 \text{ m}$$

$$A_{e,\max} = 14.7 \times 10^3 \text{ m}^2$$

$$A_{e,1} = 5.8 \times 10^3 \text{ m}^2$$

$$A_{e,1}/A_{e,\max} = 0.39$$

$$\frac{A_e}{10^3}, \text{ m}^2$$



From figure 2,

$$K_S = 0.65 \frac{\sqrt{A_{e,\max}}}{l^{3/4} l_e^{1/4}} = 0.68$$

## APPENDIX B

Propagation factors are obtained from equations (3) to (5) and figure 7.

$$M_e = \frac{1}{\sin(\gamma + \cot^{-1} \sqrt{M^2 - 1})} = 1.39 \quad K_d = 0.99$$

$$d_x = K_d \left( \frac{h}{\sqrt{M_e^2 - 1}} \right) = 37.2 \text{ km} \quad K_p = 1.40$$

$$h_e = h \cos \gamma + d_x \sin \gamma = 50.2 \text{ km} \quad K_t = 0.73$$

Impact point = 32.9 +  $d_x$  = 69.3 km from launch

The signature is calculated as follows:

$$\Delta p_{\max} = K_p K_R \sqrt{p_v p_g} (M^2 - 1)^{1/8} h_e^{-3/4} l^{3/4} K_S = 184 \text{ N/m}^2$$

$$\Delta t = K_t \frac{3.42}{a_v} \frac{M}{(M^2 - 1)^{3/8}} h_e^{1/4} l^{3/4} K_S = 3.90 \text{ sec}$$

The reader may be concerned that the effective-area curve terminates at a point where the area is still growing. This, however, does not cause any real difficulty. The major compression of the airflow about this shape takes place in the first two-thirds of the chosen effective body length. Beyond that point only relatively mild compressions or expansions occur. For example, if the shape given in reference 9 were extended along the dashed line (which appears to be a reasonable assumption) to an effective length 50 percent greater than the original effective length, the signature overpressure and duration would be unchanged. Also, the chosen effective length  $l_e$  does not in this case begin at the origin of the area plot.

## REFERENCES

1. Carlson, H. W.; and Maglieri, D. J.: Review of Sonic-Boom Generation Theory and Prediction Methods. J. Acoust. Soc. America, vol. 51, no. 2, pt. 3, Feb. 1972, pp. 675-685.
2. Hayes, Wallace D.; and Runyan, Harry L., Jr.: Sonic-Boom Propagation Through a Stratified Atmosphere. J. Acoust. Soc. America, vol. 51, no. 2, pt. 3, Feb. 1972, pp. 695-701.
3. Holloway, Paul F.; Wilhold, Gilbert A.; Jones, Jess H.; Garcia, Frank, Jr.; and Hicks, Raymond M.: Shuttle Sonic Boom - Technology and Predictions. AIAA Paper No. 73-1039, Oct. 1973.
4. Carlson, Harry W.; and Mack, Robert J.: A Study of the Sonic-Boom Characteristics of a Blunt Body at a Mach Number of 4.14. NASA TP-1015, 1977.
5. Hayes, Wallace D.; Haefeli, Rudolph C.; and Kulsrud, H. E.: Sonic Boom Propagation in a Stratified Atmosphere, With Computer Program. NASA CR-1299, 1969.
6. Carlson, Harry W.: Correlation of Sonic-Boom Theory With Wind-Tunnel and Flight Measurements. NASA TR R-213, 1964.
7. Kane, Edward J.; and Palmer, Thomas Y.: Meteorological Aspects of the Sonic Boom. SRDS Rep. No. RD64-160 (AD 610 463), FAA, Sept. 1964.
8. Hubbard, Harvey H.; Maglieri, Domenic J.; Huckel, Vera; and Hilton, David A. (With appendix by Harry W. Carlson): Ground Measurements of Sonic-Boom Pressures for the Altitude Range of 10,000 to 75,000 Feet. NASA TR R-198, 1964. (Supersedes NASA TM X-633.)
9. Williams, M. E. L.; and Page, N. M.: Measurement of Sonic Boom From Concorde - 002 Australia 1972. R&D Rep. No. 896, Dep. Civ. Aviat., Commonwealth Australia, Aug. 1972.
10. Maglieri, Domenic J.; Huckel, Vera; and Henderson, Herbert R.: Sonic-Boom Measurements for SR-71 Aircraft Operating at Mach Numbers to 3.0 and Altitudes to 24 384 Meters. NASA TN D-6823, 1972.
11. Hilton, David A.; Henderson, Herbert R.; and McKinney, Royce: Sonic-Boom Ground-Pressure Measurements From Apollo 15. NASA TN D-6950, 1972.
12. Henderson, Herbert R.; and Hilton, David A.: Sonic-Boom Ground Pressure Measurements From the Launch and Reentry of Apollo 16. NASA TN D-7606, 1974.
13. Henderson, Herbert R.; and Hilton, David A.: Sonic-Boom Measurements in the Focus Region During the Ascent of Apollo 17. NASA TN D-7806, 1974.

14. Sonic Boom Experiments at Edwards Air Force Base. NSBEO-1-67 (Contract AF 49(638)-1758), CFSTI, U.S. Dep. Com., July 28, 1967.
15. Garrick, I. E.; and Maglieri, D. J.: A Summary of Results on Sonic-Boom Pressure-Signature Variations Associated With Atmospheric Conditions. NASA TN D-4588, 1968.
16. Taylor, John W. R., ed.: Jane's All the World's Aircraft. McGraw-Hill Book Co., c.1970.
17. Hicks, Raymond M.; and Mendoza, Joel P.: Pressure Signatures for a .00053 Scale Model of the Saturn V-Apollo Launch Vehicle With Simulated Exhaust Plumes. NASA TM X-62,129, 1973.

### Basic information required

Aircraft geometry (for aircraft not covered  
by shape-factor charts)

Operating conditions

Mach number

Altitude

Weight

Flight-path angle

Atmospheric data

Ambient pressure

Sound speed

### Data obtained

Bow-shock overpressure  $\Delta p_{\max}$

Signature duration  $\Delta t$

Ground impact point

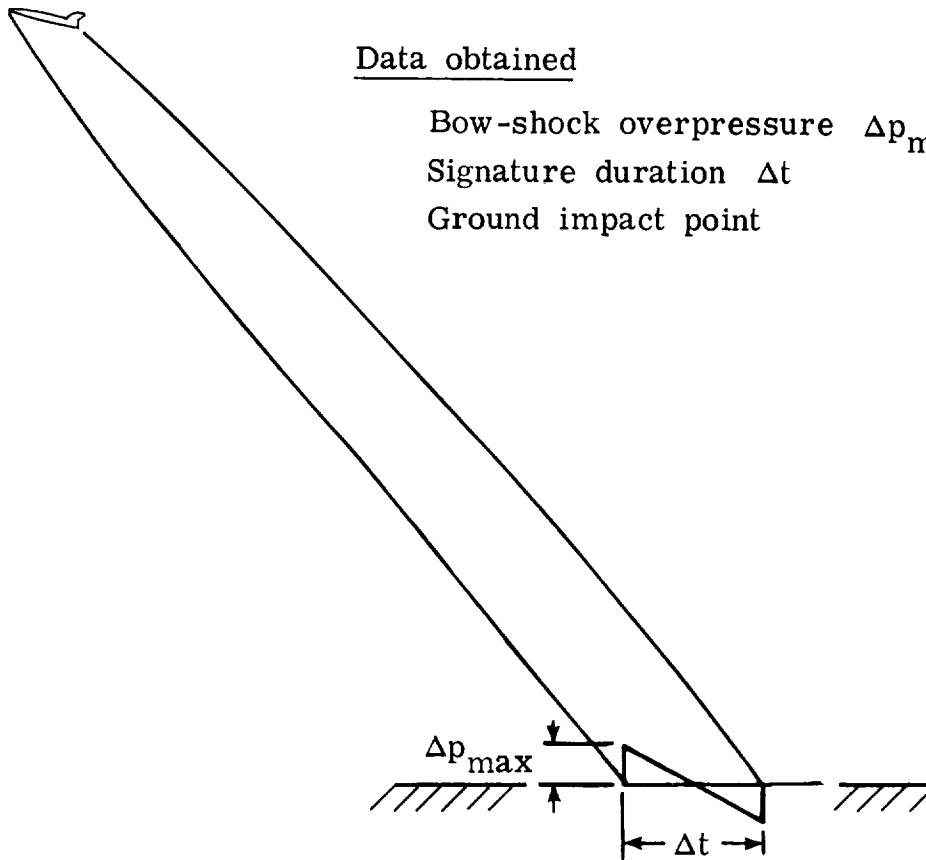


Figure 1.- Information required and data provided by simplified sonic-boom prediction method.

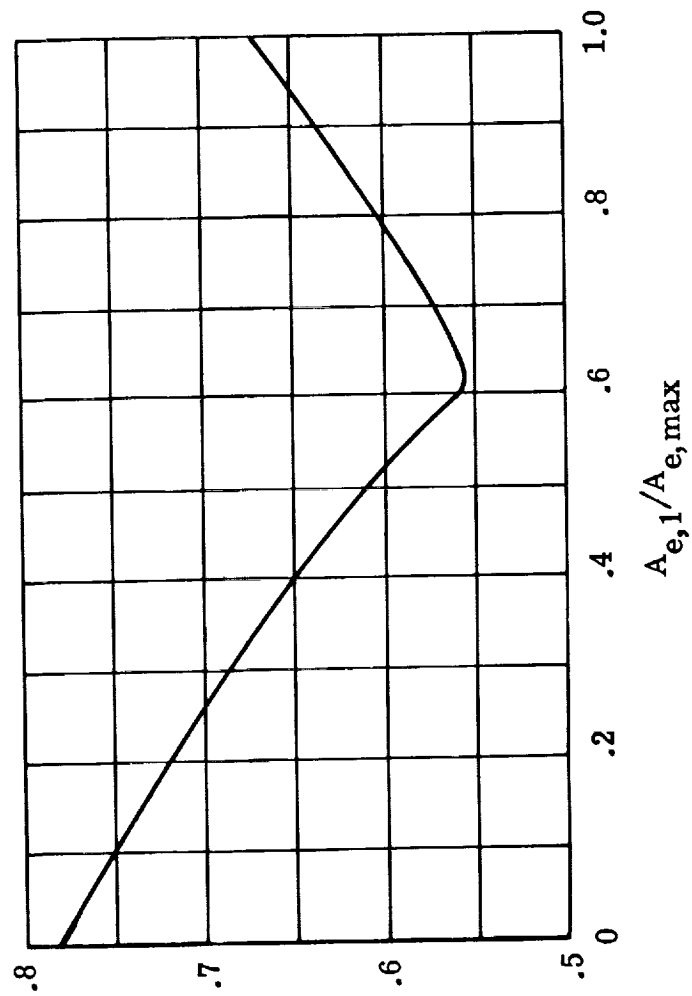
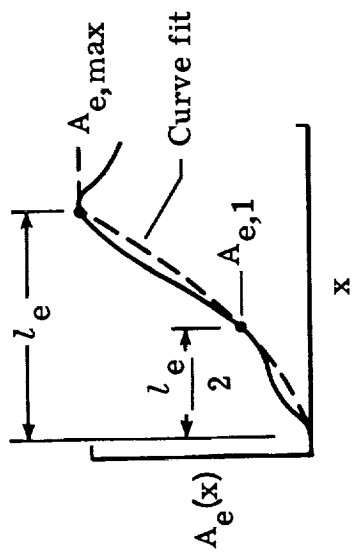


Figure 2.- Shape-factor parameter.

$$\frac{K_S}{\left( \frac{\sqrt{A_{e,max}}}{l_e^{3/4} l_e^{1/4}} \right)}$$

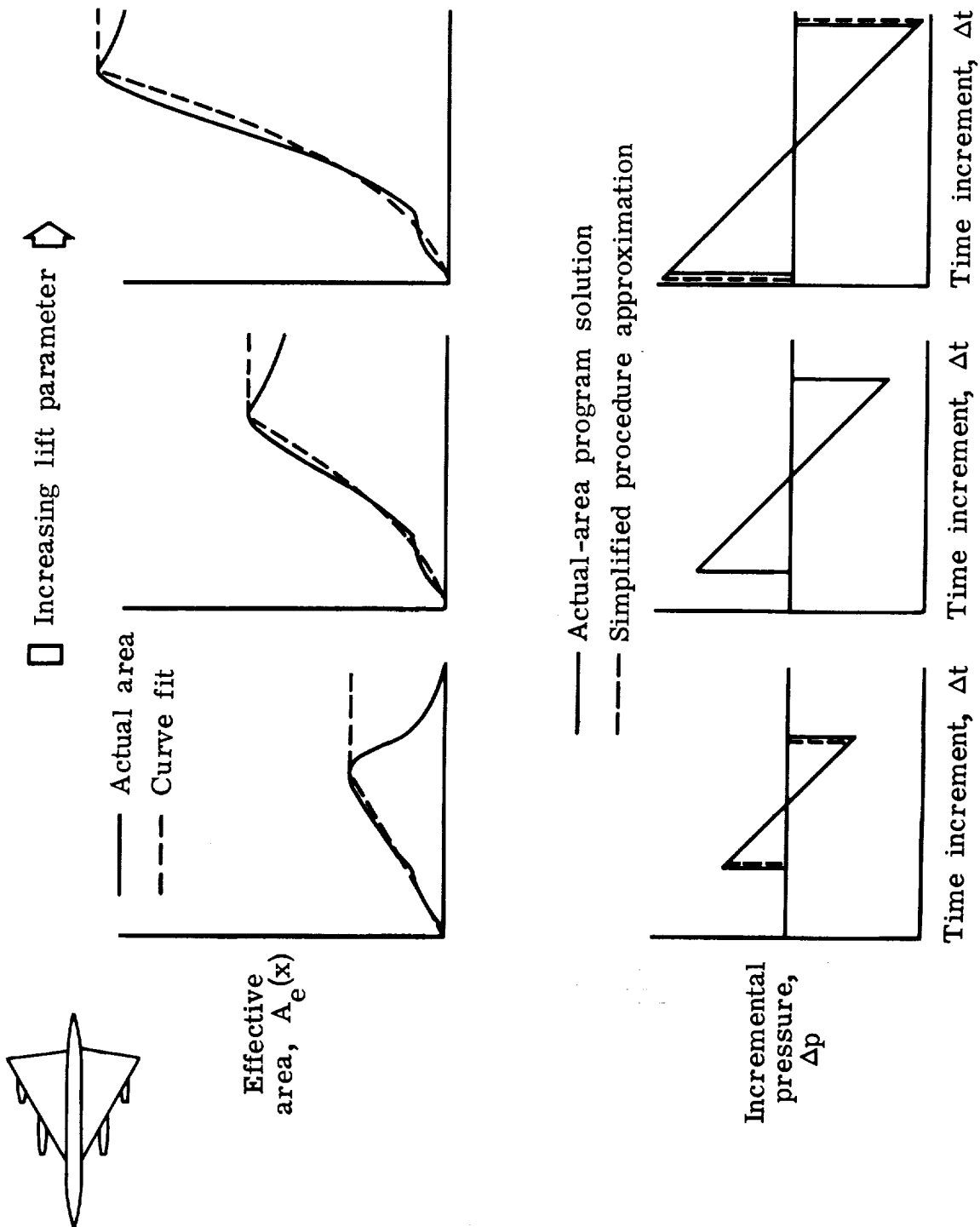
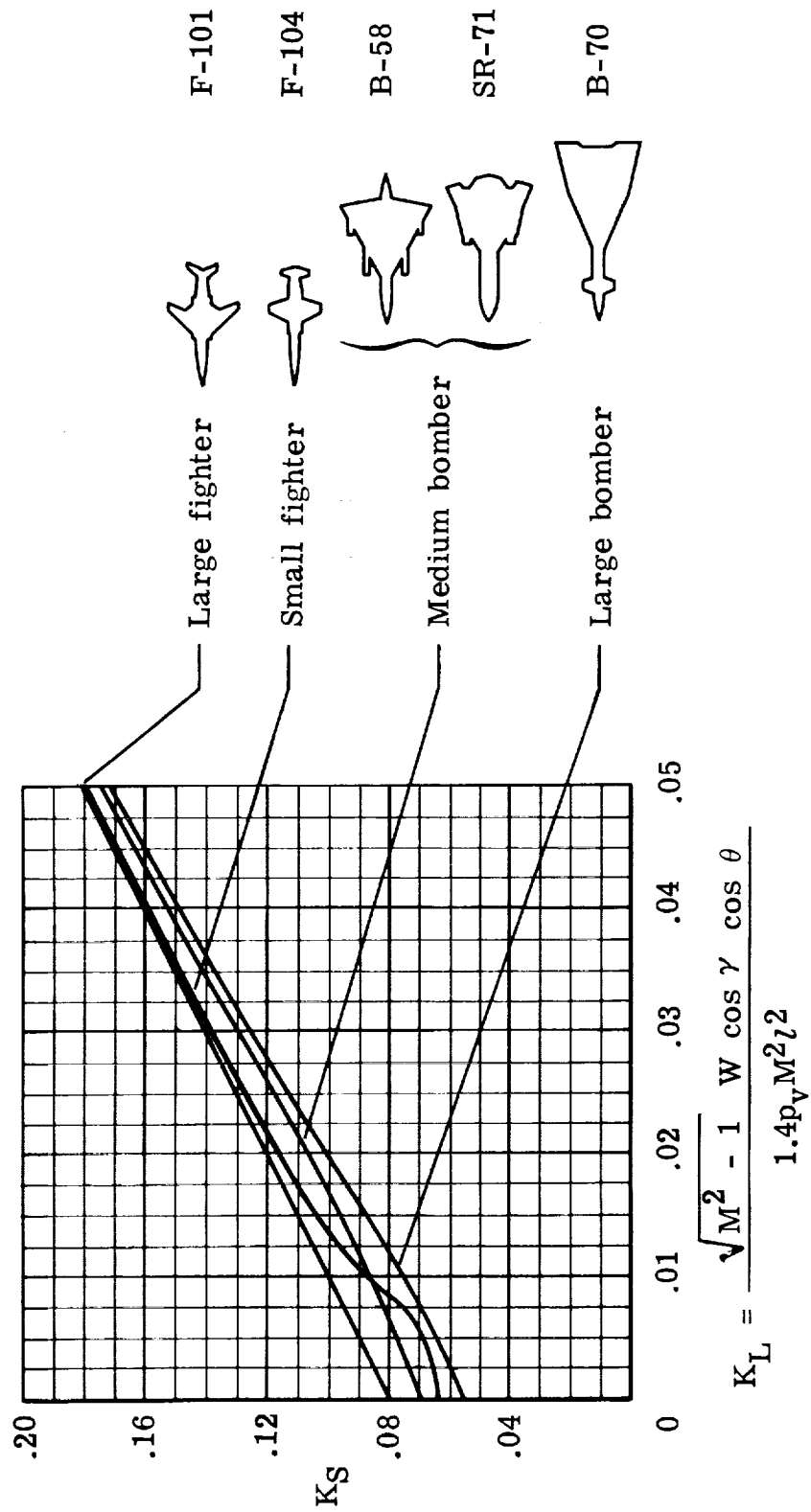


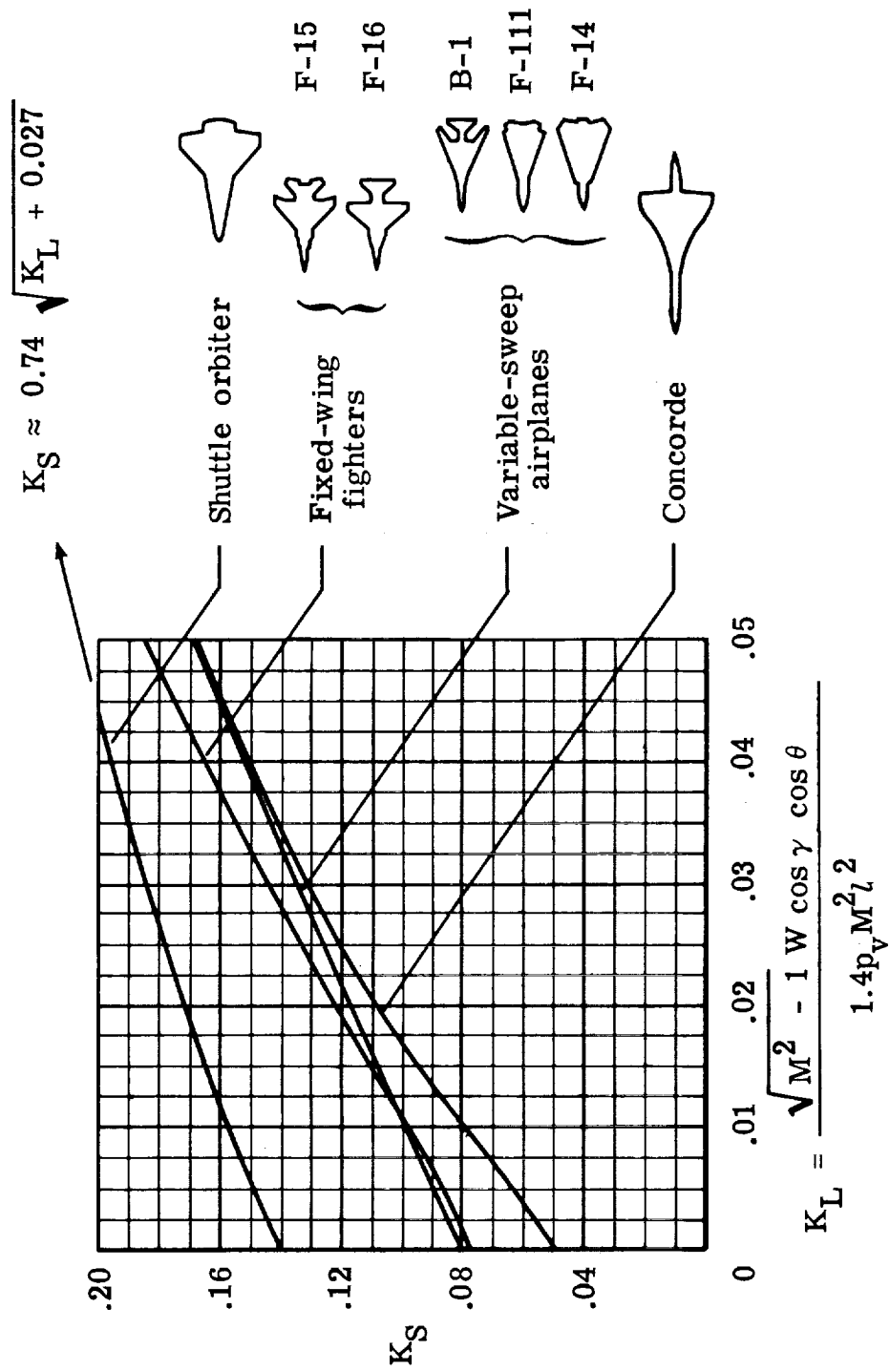
Figure 3.- Comparison of simplified procedure approximation with computer program results for actual effective areas.



(a) Sonic-boom test airplanes.

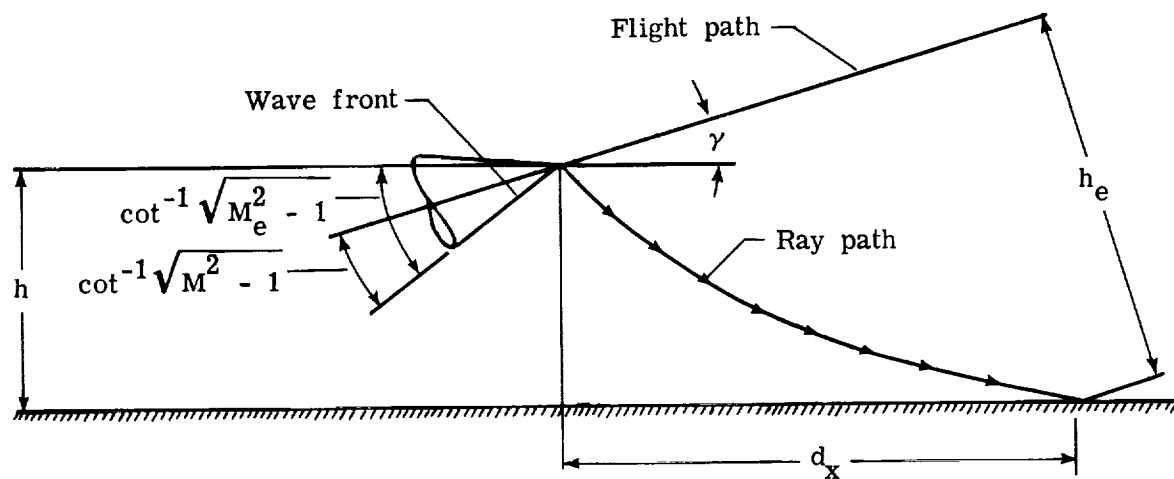
Figure 4.- Representative aircraft shape factors.



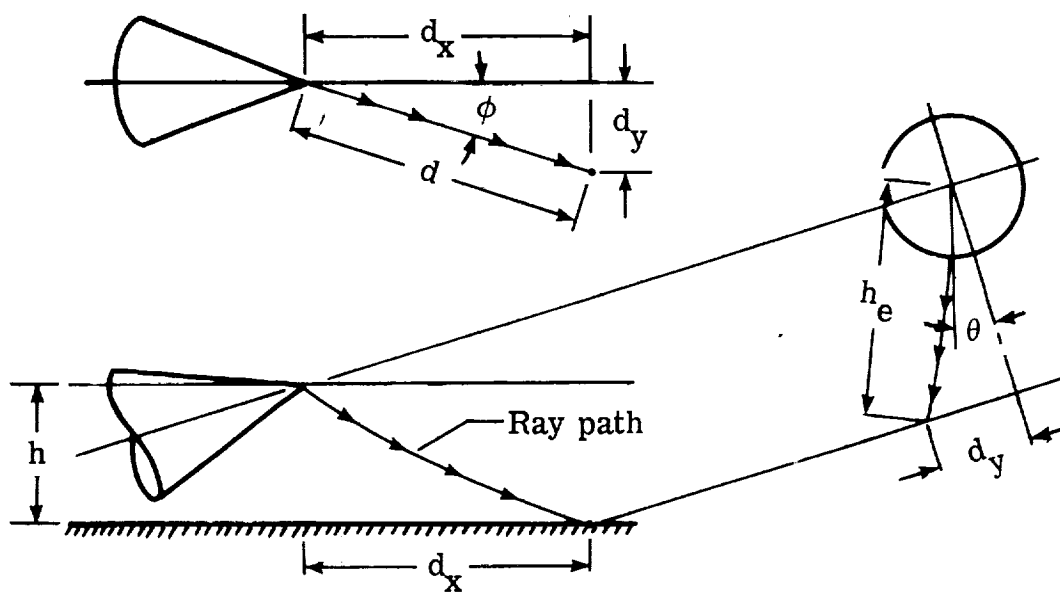


(b) Contemporary aircraft.

Figure 4.- Concluded.

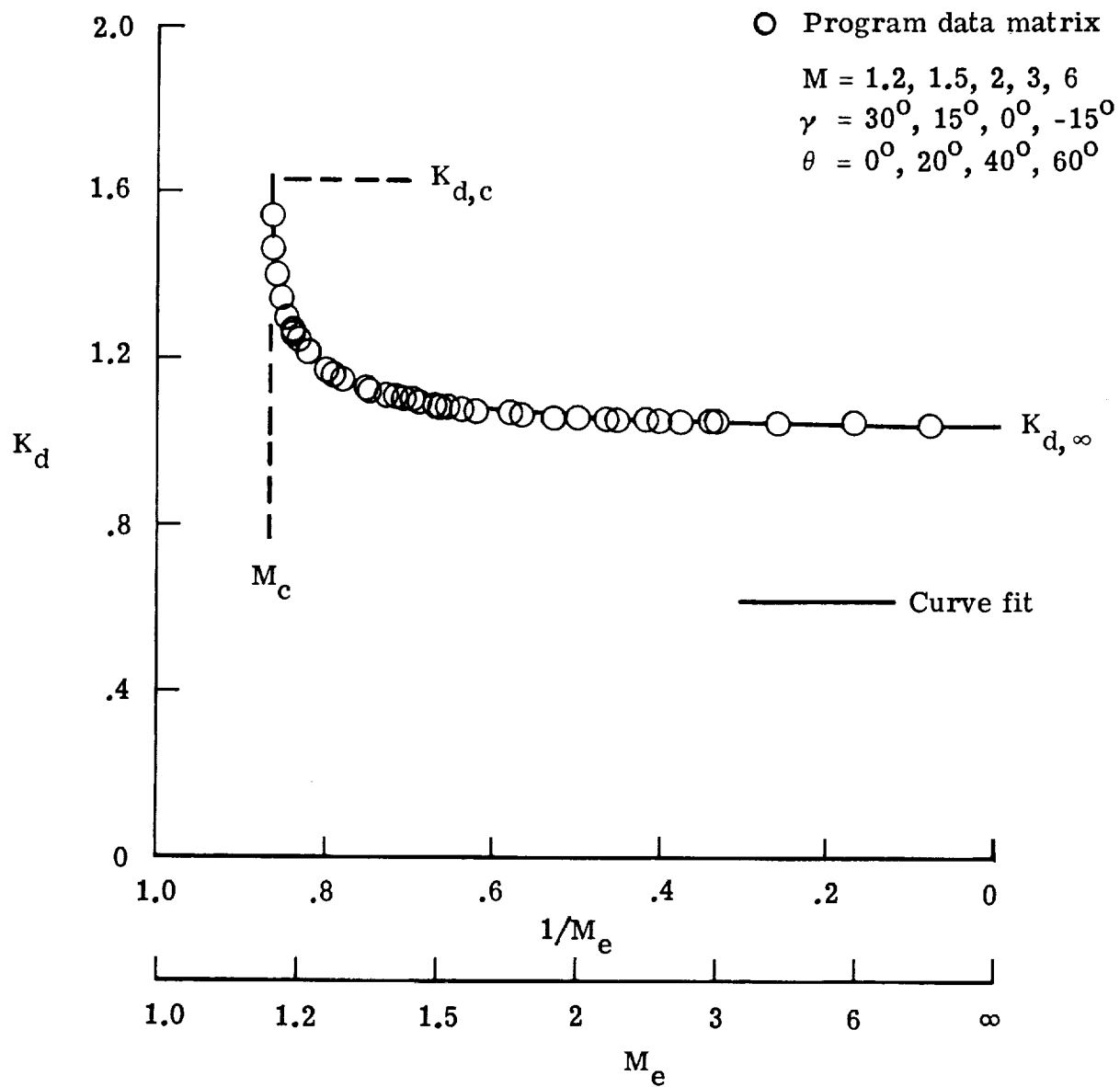


(a) On-track.



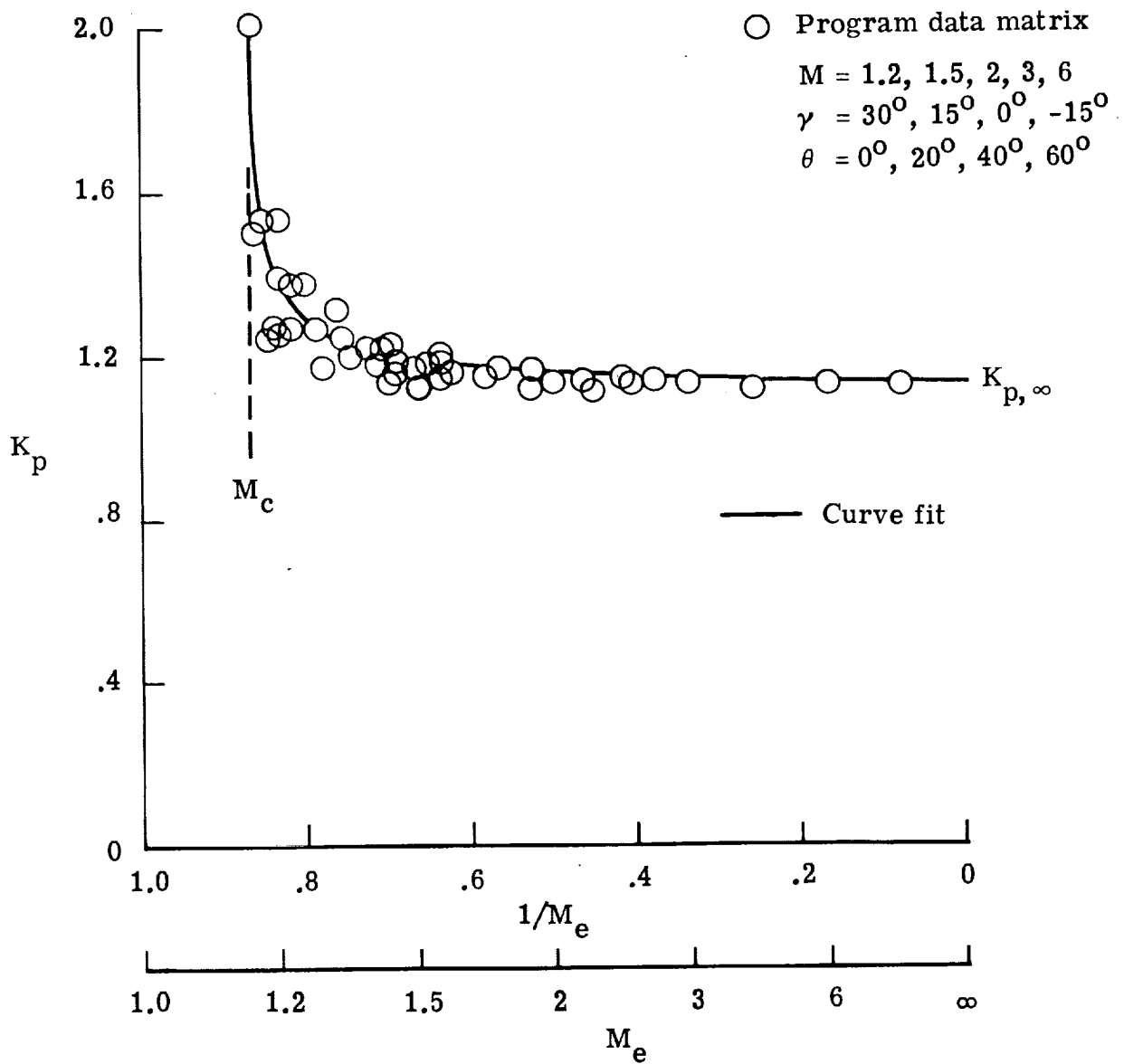
(b) Off-track.

Figure 5.- Propagation geometric parameters.



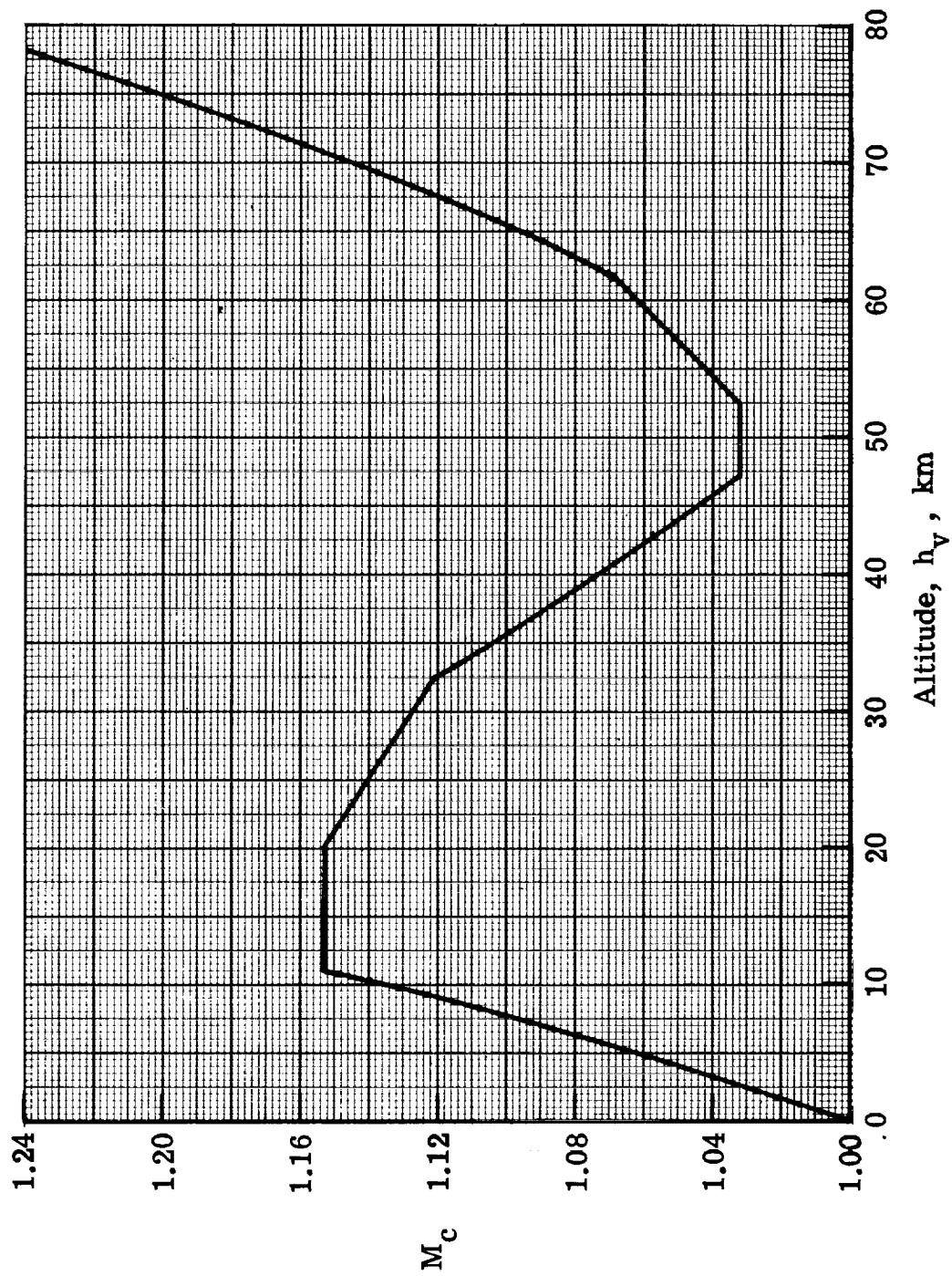
(a) Ray-path distance factor.

Figure 6.- Illustration of use of effective Mach number in reduction of atmospheric propagation program data.  $h_v = 20$  km.



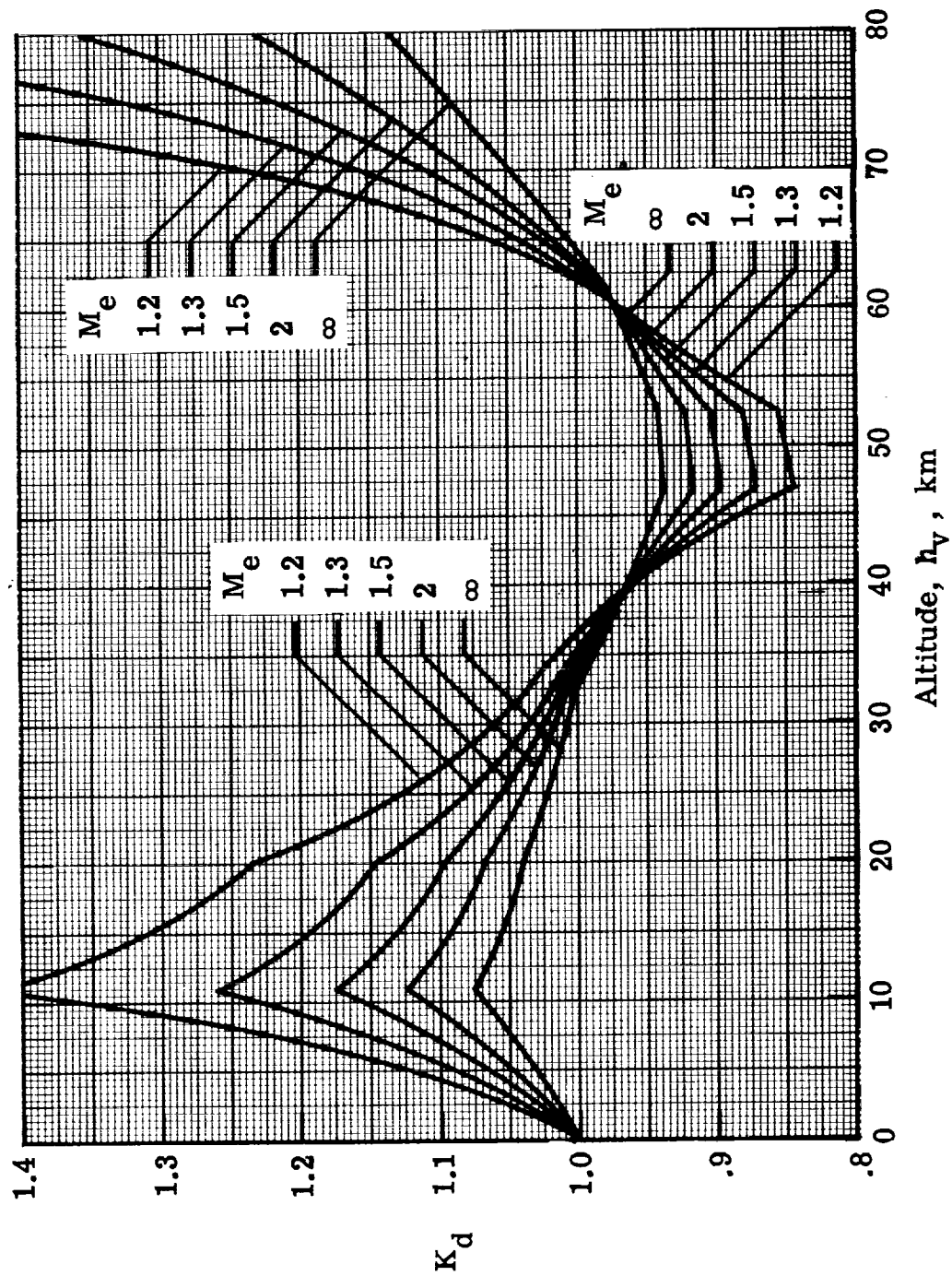
(b) Pressure amplification factor.

Figure 6.- Concluded.



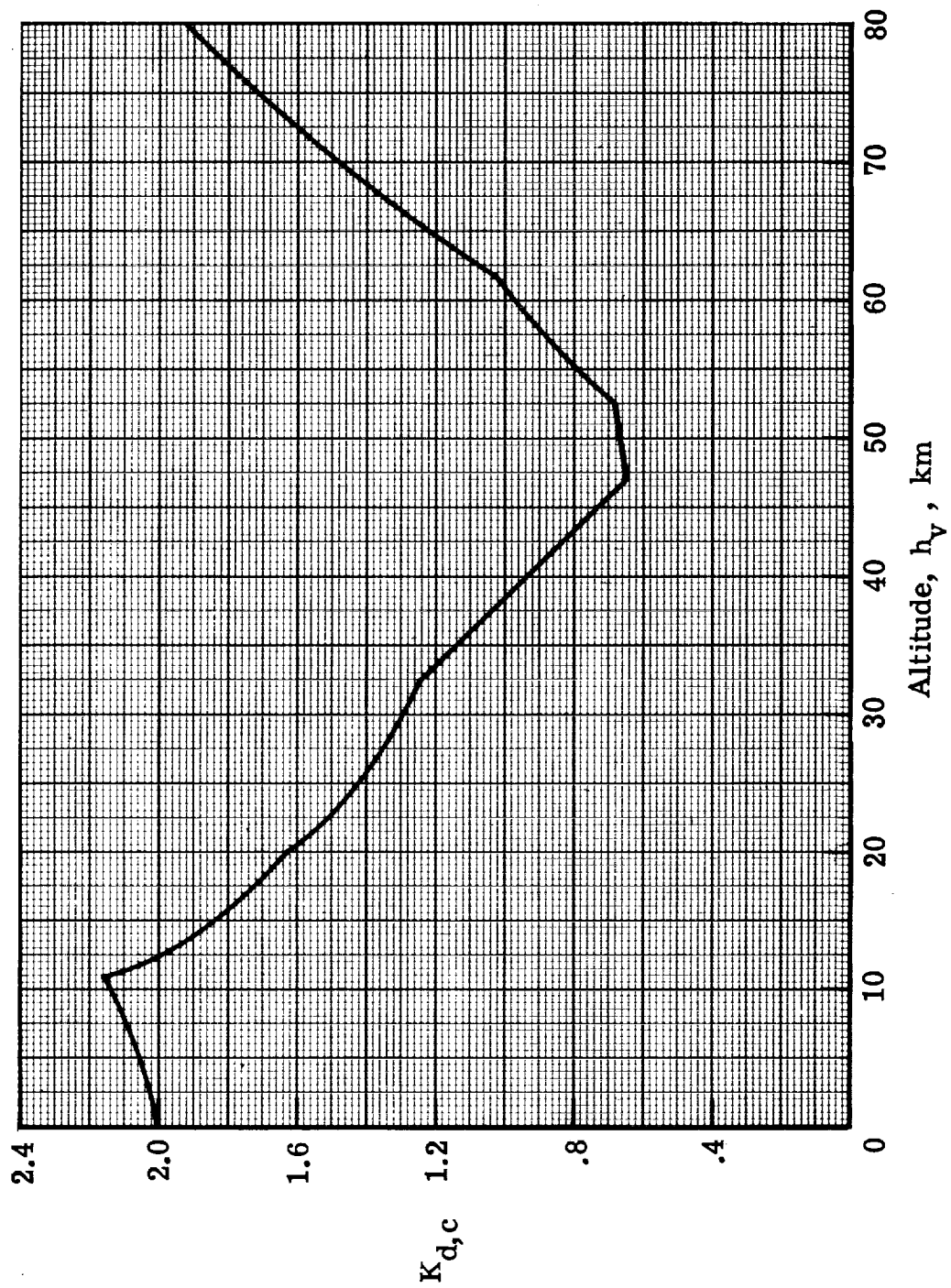
(a) Cutoff Mach number  $M_c$ .

Figure 7.- Atmospheric-factor charts.



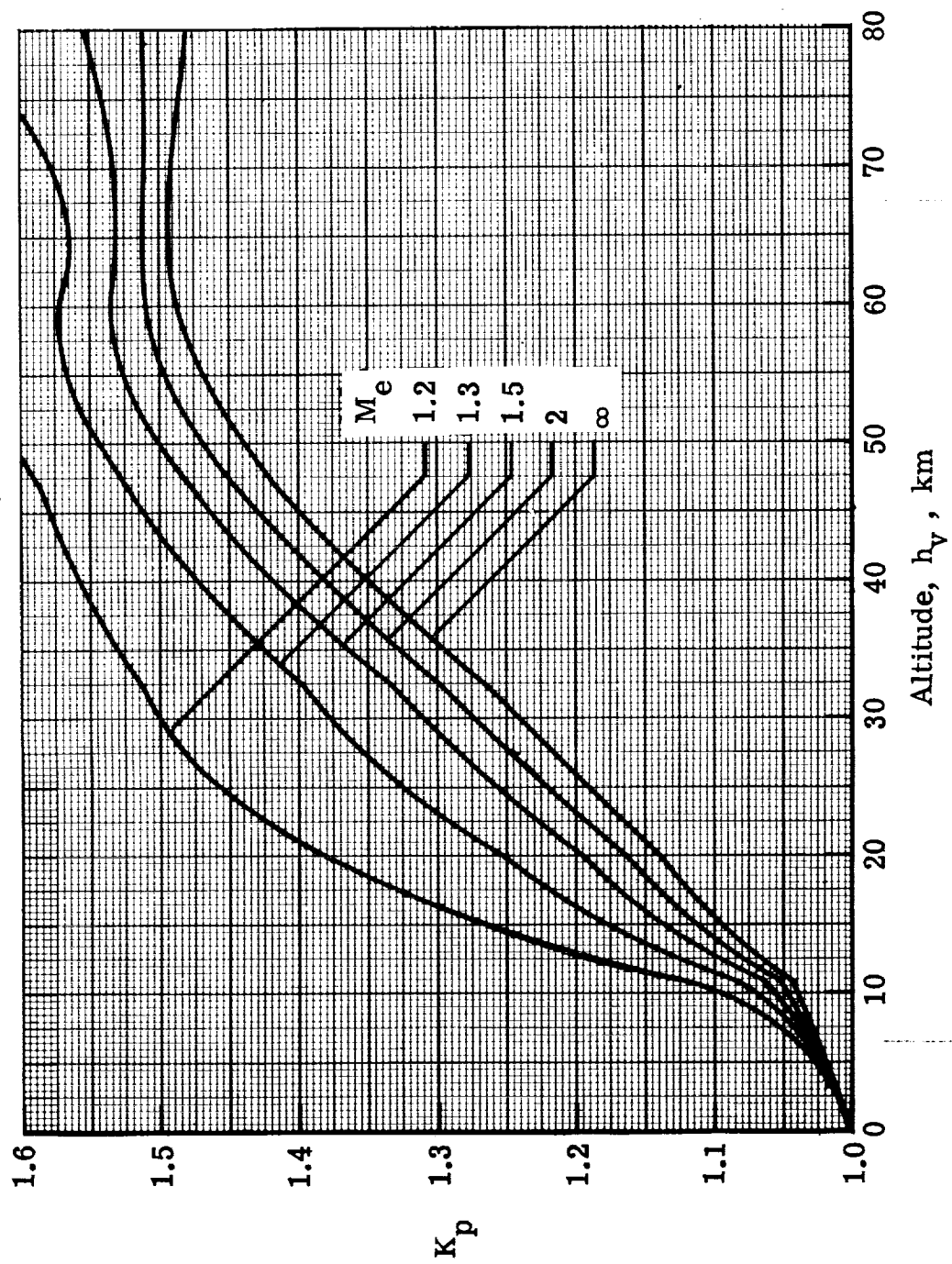
(b) Ray-path distance factor  $K_d$ .

Figure 7.- Continued.



(c) Cutoff ray-path distance factor  $K_{d,c}$ .

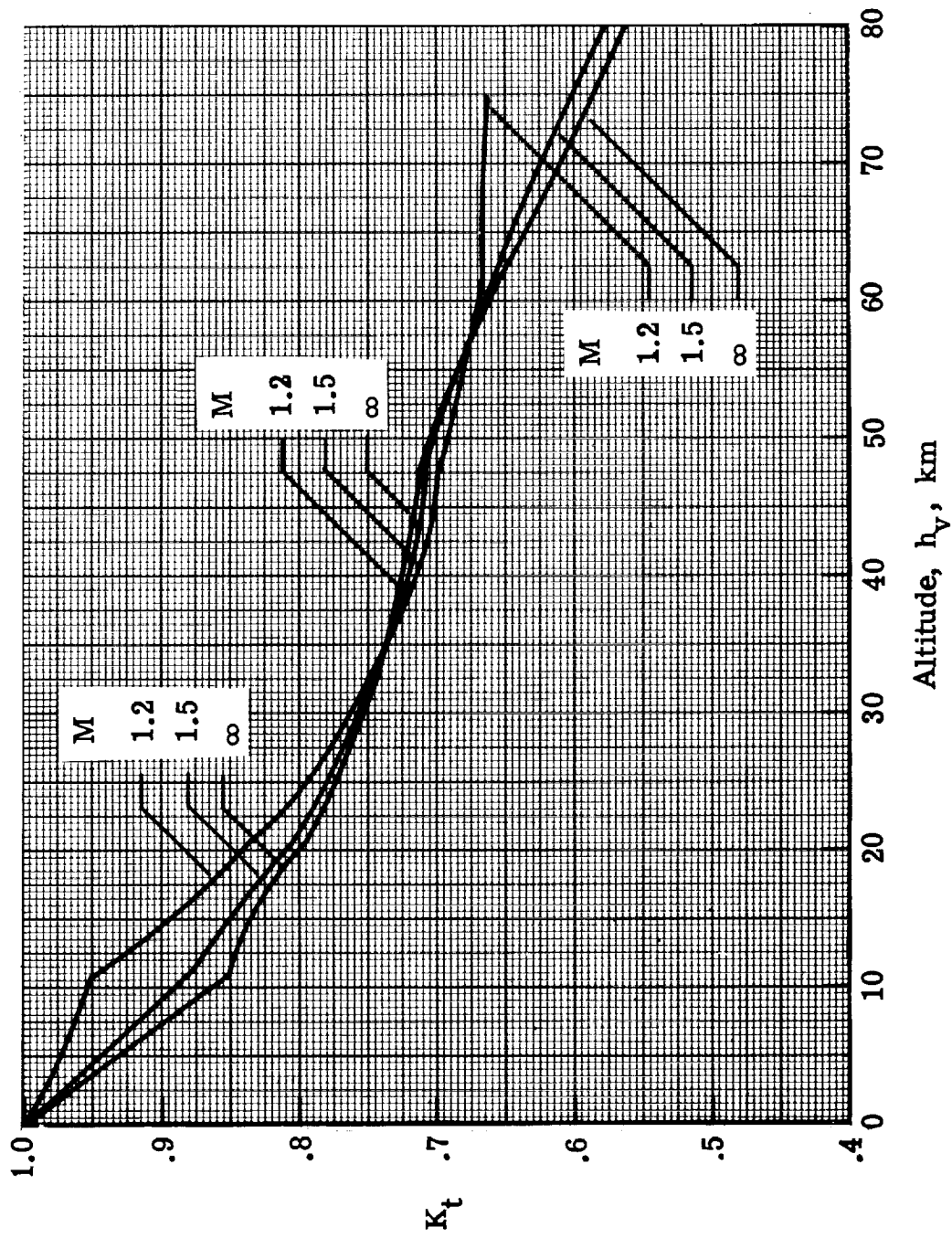
Figure 7.- Continued.



(d) Pressure amplification factor  $K_p$ .

Figure 7.- Continued.





(e) Signature duration factor  $K_t$ .

Figure 7.- Concluded.

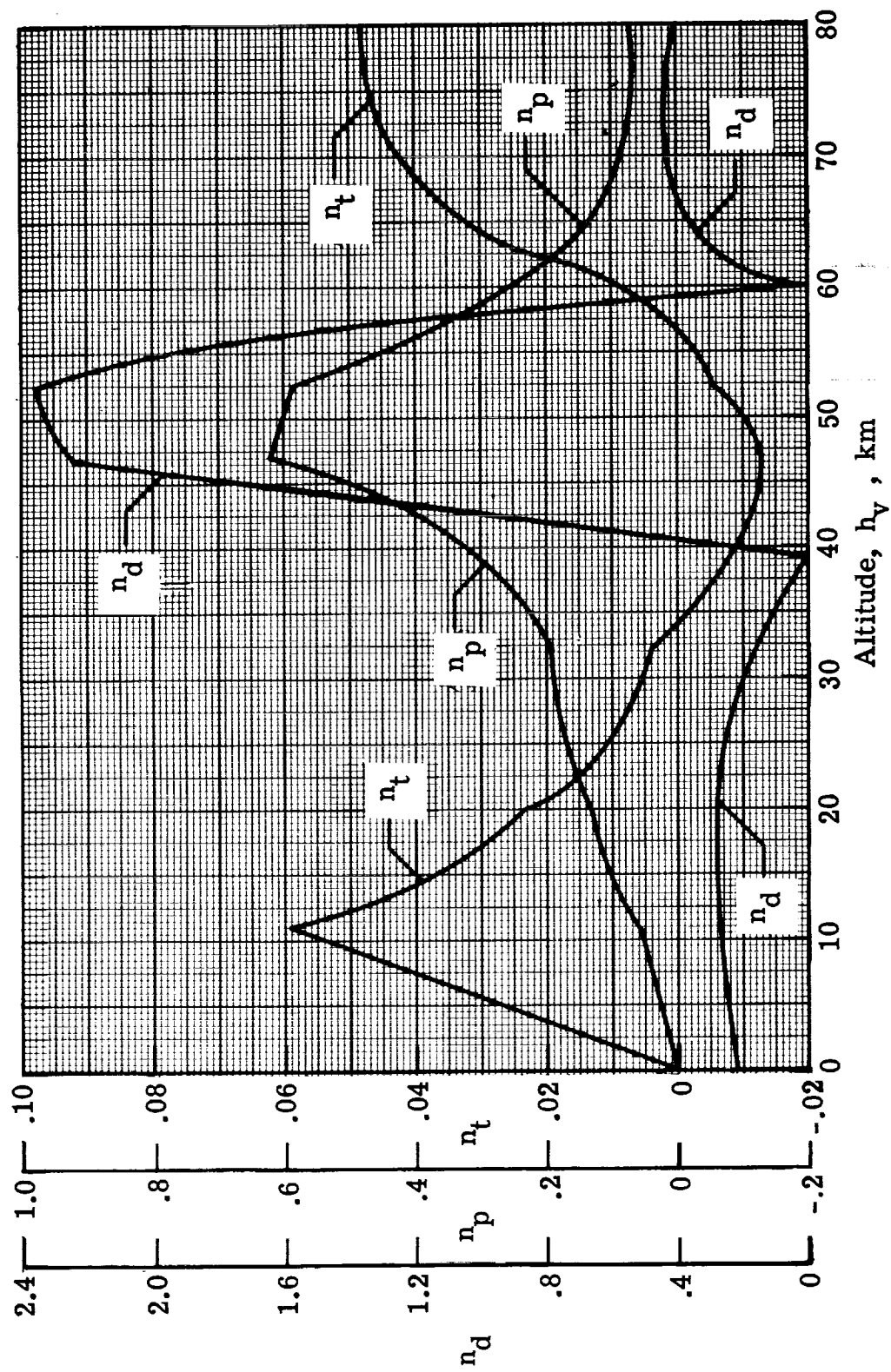


Figure 8.- Atmospheric-factor curve-fit exponents.

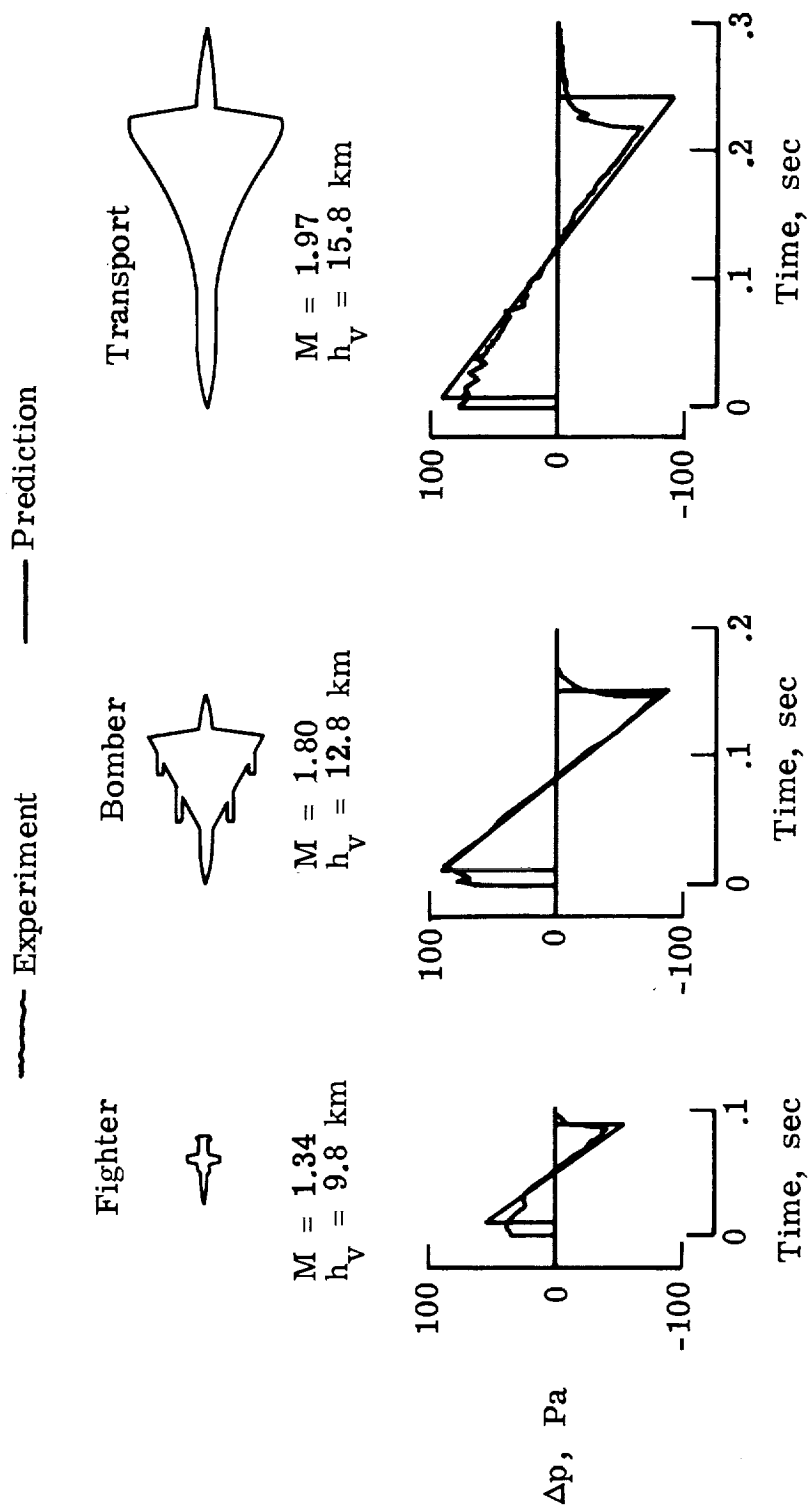


Figure 9.- Correlation of predictions with measurements covering a range of airplane types.

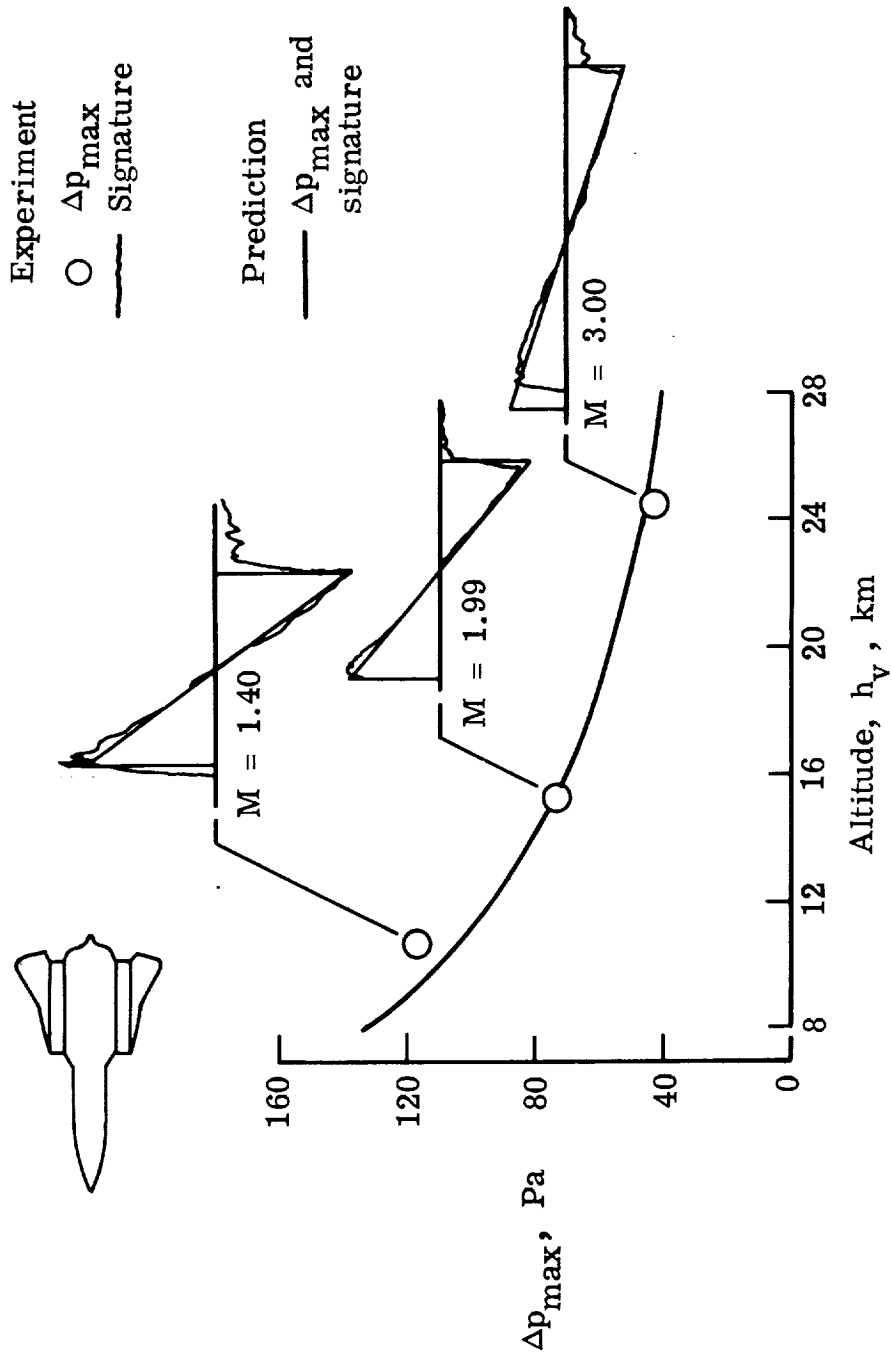


Figure 10.- Correlation of predictions with measurements covering a range of altitude for a reconnaissance airplane.

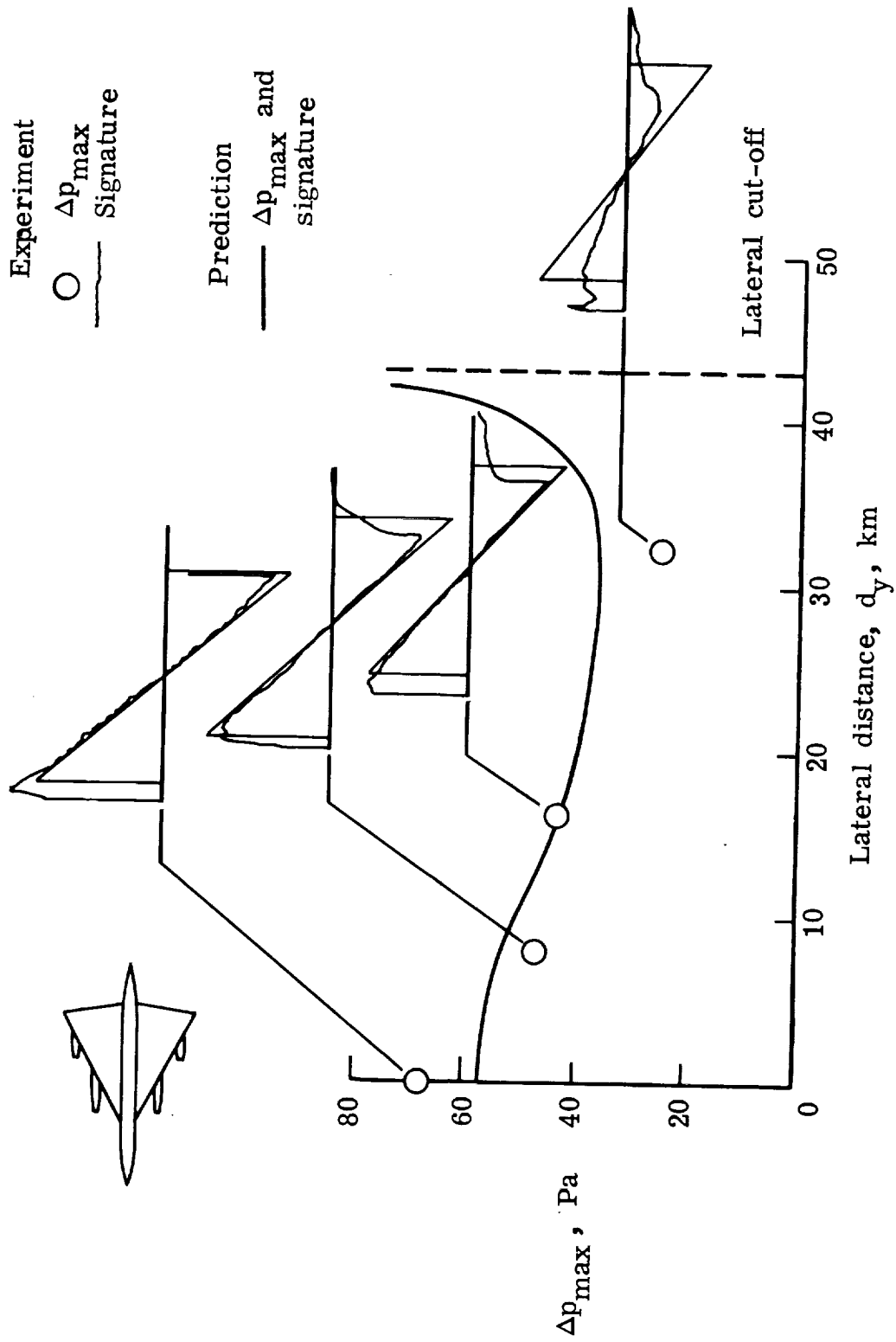


Figure 11.- Correlation of predictions with measurements covering a range of lateral distances for a bomber airplane.  $M = 2.0$ ,  $h_V = 18.5$  km.

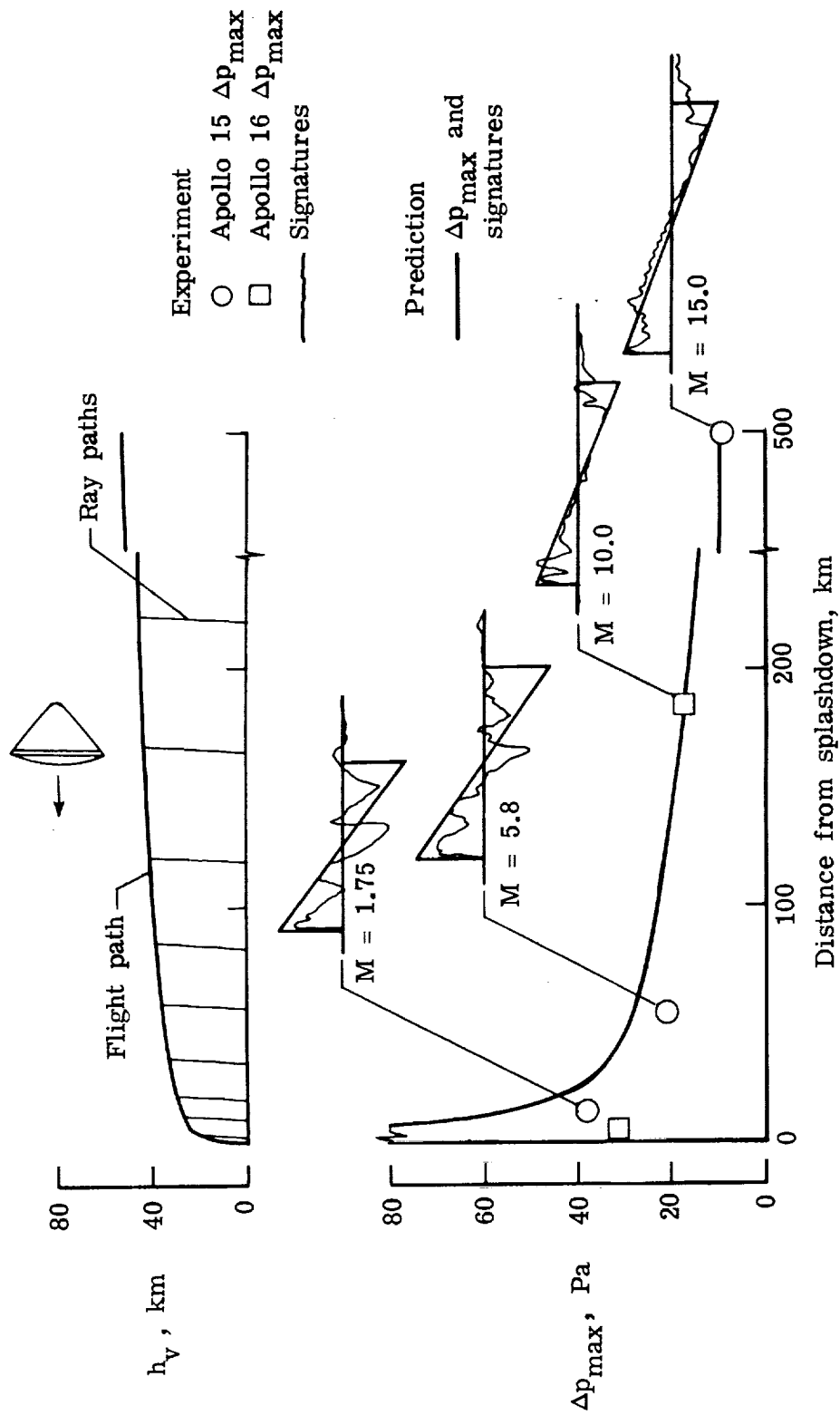


Figure 12.- Correlation of predictions with measurements made during reentries of Apollo 15 and 16.

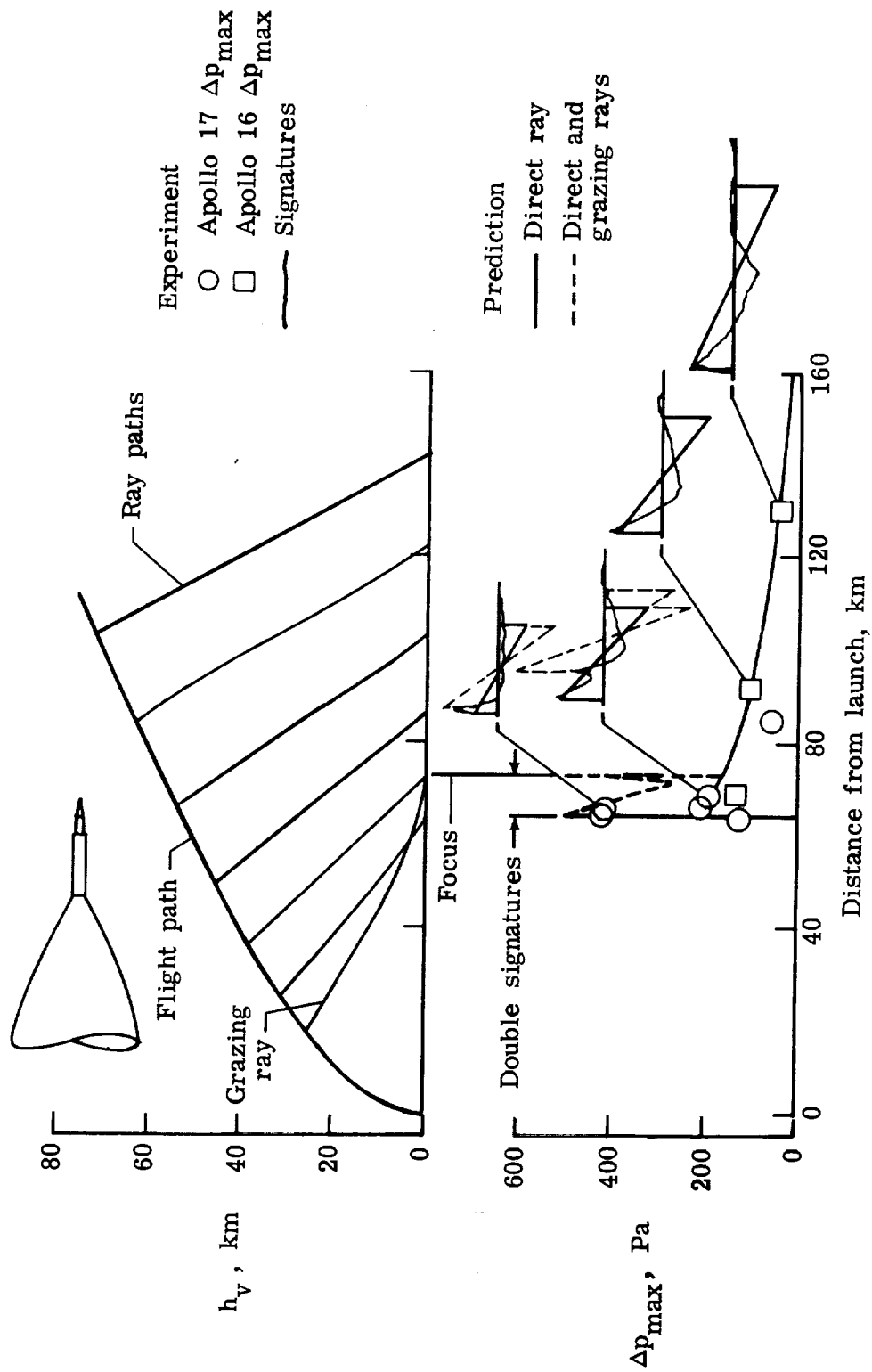
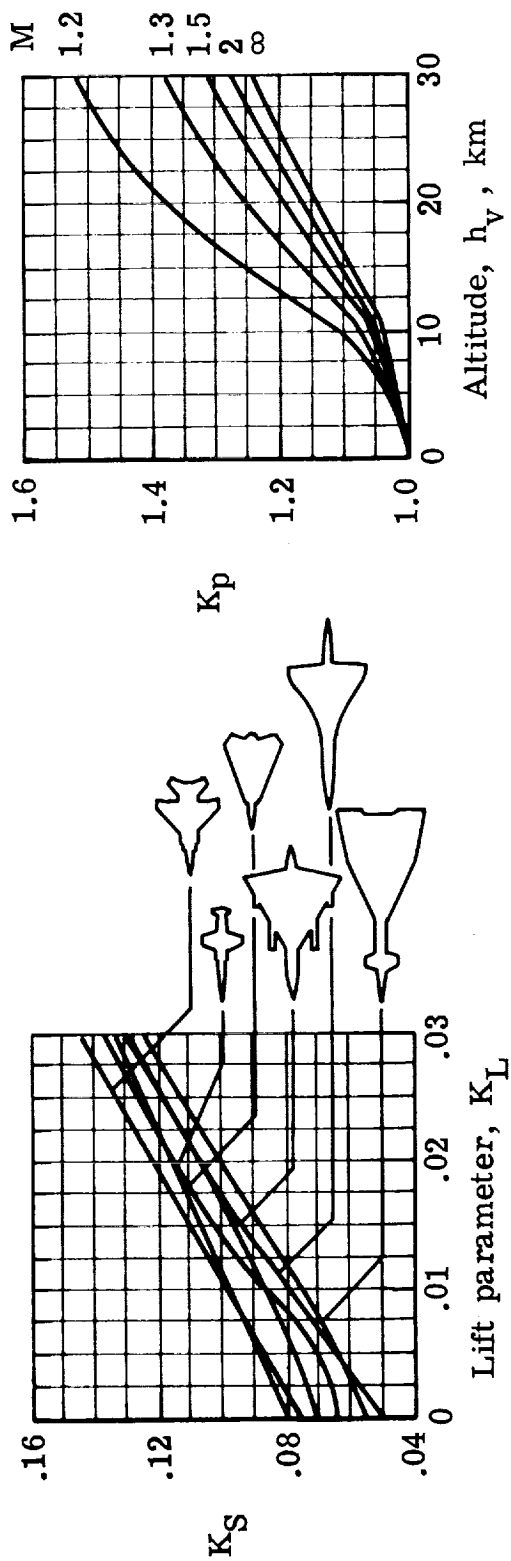


Figure 13.- Correlation of predictions with measurements made during ascents of Apollo 16 and 17.



(1) Enter lift parameter  $K_L$

$$K_L = \frac{\sqrt{M^2 - 1} W}{1.4 p_v M^2 l^2}$$

Select shape factor  $K_S$

(2) Enter altitude  $h_v$  and

Mach number  $M$

Read pressure amplification  
factor  $K_p$

(3) Calculate bow-shock overpressure

$$\Delta p_{\max} = 2 K_p K_S \sqrt{p_v p_g} (M^2 - 1)^{1/8} h^{-3/4} l^{3/4}$$

Figure 14.- Super-simplified sonic-boom prediction method for on-track bow-shock overpressure of conventional airplanes in level flight.



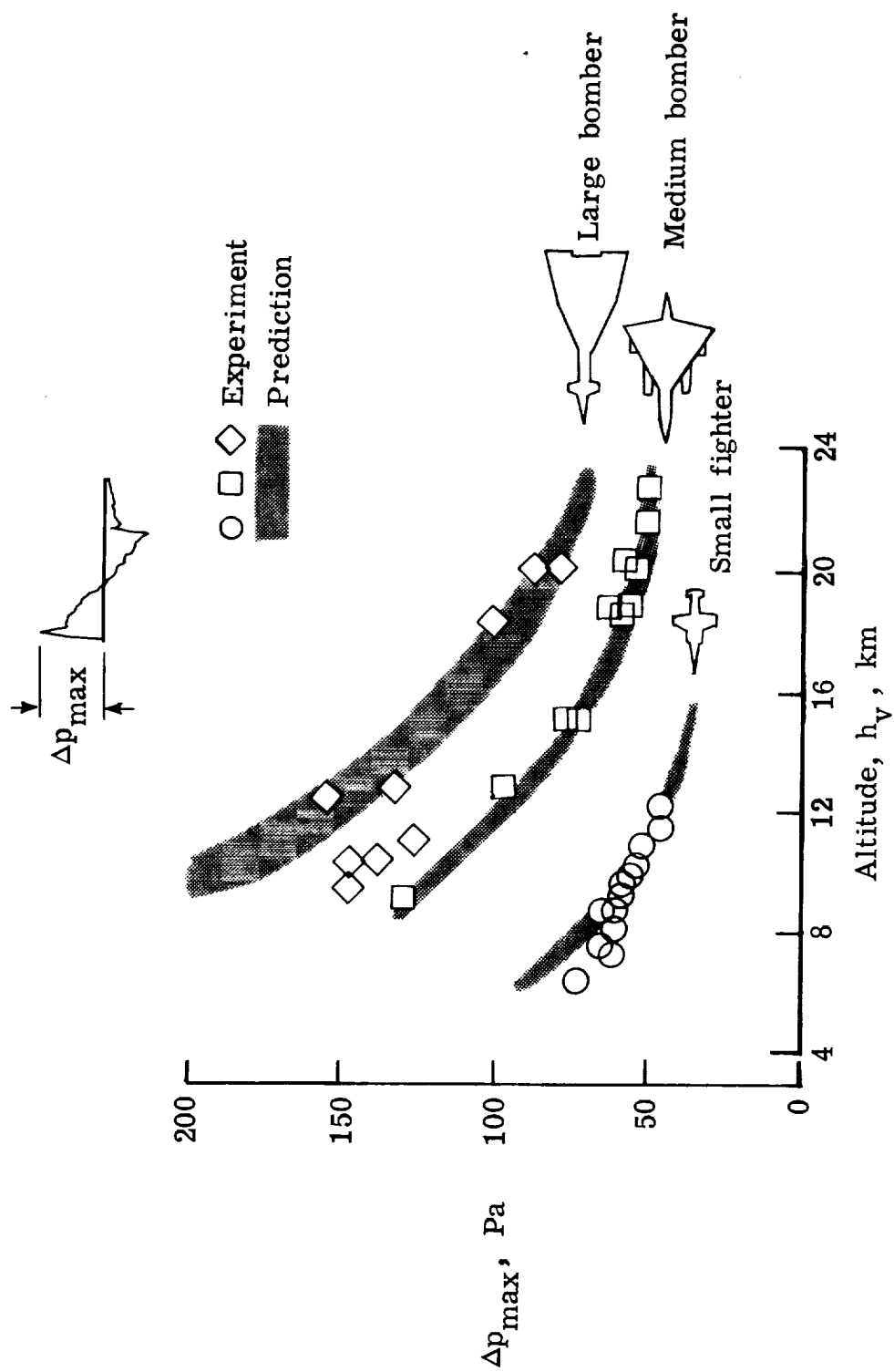


Figure 15.- Correlation of on-track bow-shock overpressure predictions with measurements.





1. Report No. NASA TP-1122		2. Government Accession No.		3. Recipient's Catalog No.	
4. Title and Subtitle  SIMPLIFIED SONIC-BOOM PREDICTION				5. Report Date March 1978	
				6. Performing Organization Code	
7. Author(s) Harry W. Carlson				8. Performing Organization Report No. L-11794	
9. Performing Organization Name and Address  NASA Langley Research Center Hampton, VA 23665				10. Work Unit No. 743-04-31-01	
				11. Contract or Grant No.	
12. Sponsoring Agency Name and Address  National Aeronautics and Space Administration Washington, DC 20546				13. Type of Report and Period Covered Technical Paper	
				14. Sponsoring Agency Code	
15. Supplementary Notes					
16. Abstract  <p>A simplified method for the calculation of sonic-boom characteristics for a wide variety of supersonic airplane configurations and spacecraft operating at altitudes up to 76 km has been developed. Sonic-boom overpressures and signature duration may be predicted for the entire affected ground area for vehicles in level flight or in moderate climbing or descending flight paths. The outlined procedure relies to a great extent on the use of charts to provide generation and propagation factors for use in relatively simple expressions for signature calculation. Computational requirements can be met by hand-held scientific calculators, or even by slide rules. A variety of correlations of predicted and measured sonic-boom data for airplanes and spacecraft serve to demonstrate the applicability of the simplified method.</p>					
17. Key Words (Suggested by Author(s))  Sonic boom Shock-wave noise			18. Distribution Statement  Unclassified - Unlimited  Subject Category 02		
19. Security Classif. (of this report) Unclassified	20. Security Classif. (of this page) Unclassified	21. No. of Pages 47	22. Price* \$4.50		

\* For sale by the National Technical Information Service, Springfield, Virginia 22161

NASA-Langley, 1978